Coordination of transcriptional and translational regulations in human cells infected by *Listeria monocytogenes*

Vinko Besic[1], Fatemeh Habibolahi[1,2*], Benoît Noël[1,2*], Sebastian Rupp[1], Auguste Genovesio[2] and Alice Lebreton[1,4,‡]

[1] Bacterial Infection & RNA Destiny group, Institut de biologie de l'ENS (IBENS), Département de biologie, École normale supérieure, CNRS, INSERM, PSL University, 75005 Paris, France.

[2] Computational Biology and Bioinformatics group, Institut de biologie de l'ENS (IBENS), Département de biologie, École normale supérieure, CNRS, INSERM, PSL University, 75005 Paris, France.

[4] INRA, IBENS, 75005 Paris, France.

[*] Equal contribution

[‡] Correspondence to: alice.lebreton@ens.fr

Abstract

The invasion of mammalian cells by intracellular bacterial pathogens reshuffles their gene expression and functions; however, we lack dynamic insight into the distinct control levels that shape the host response. By comparing ribosome profiling and transcriptome data, we have addressed the respective contribution of transcriptional and translational regulations during a time-course of infection of human intestinal epithelial cells by an epidemic strain of *Listeria monocytogenes*. Upregulations were dominated by early transcriptional activation of pro-inflammatory genes, whereas translation inhibition appeared as the major source of downregulations. Instead of a widespread shutoff, translation inhibition affected durably and specifically transcripts encoding components of the translation machinery, and harbouring a 5'-terminal oligopyrimidine motif. Pre-silencing the most repressed target gene (*PABPC1*) slowed down the intracellular multiplication of *Listeria*, suggesting that the infected host cell can benefit from the repression of genes involved in protein synthesis and thereby better control infection.

Introduction

Invasion and proliferation of intracellular bacterial pathogens in human cells trigger drastic changes in cell functions, including their gene expression (reviewed in Cornejo, Schlaermann, & Mukherjee, 2017). For instance, the infection of cells by a variety of bacterial invaders has been described to trigger the activation of pro-inflammatory transcription factors, as well as a transient inhibition of host cap-dependent translation (reviewed in Lemaitre & Girardin, 2013). Meanwhile, the survival and multiplication of intracellular bacteria depends upon their capacity to subvert the host cell metabolism, functions and antibacterial defences, part of which can be achieved by perturbing the host gene expression (*e.g.* Niller & Minarovits, 2016).

In the past decade, due to the rise of high-resolution transcriptomic approaches, the host transcriptional response to bacterial infections has been extensively explored in a broad range of biological contexts. In contrast, few studies have investigated the perturbation of host translation at an omics scale. Previous reports however support the existence of potent regulations affecting host mRNA translation during bacterial infections. For instance, a growing number of studies have finely characterised miRNA-mediated regulation of specific host transcripts and cellular processes (Aguilar, Mano, & Eulalio, 2019; reviewed in Duval, Cossart, & Lebreton, 2017). Pathogenic bacteria can also target central host translation mechanisms, and thereby tune —positively or negatively— the production of host defence proteins (reviewed in Mohr & Sonenberg, 2012). The best described example to date is probably that of the intracellular bacterium *Legionella pneumophila* (*Lp*), which has been shown to secrete effectors that target host translation elongation and stimulate cytokine production (Fontana *et al*., 2011). In line with this, the translatome of *Lp*-infected murine macrophages has pioneered the attempts to discriminate between transcriptional and translational inputs in the fine-tuning of the inducible immune response to infection (Barry, Ingolia, & Vance, 2017). Barry *et al*. highlighted that the superinduction of cytokine mRNA transcription allows infected cells to overcome the general translation elongation blockade imposed by *Lp* effectors, and thus launch a pro-inflammatory response.

Listeria monocytogenes (*Lm*) is the foodborne cause of listeriosis, an opportunistic disease of human and cattle that can have severe consequences during pregnancy or in elderly patients. This facultative intracellular bacterium has long been a model for studying all aspects of infection biology, from host-pathogen interactions at the molecular level to *in vivo* and epidemiology studies (reviewed in Radoshevich & Cossart, 2017). How the combination of (*a*) the activity of virulence factors and (*b*) cell autonomous responses contribute to the re-organisation of cell functions has been extensively studied; however, in this model as well as in others, gene expression has mostly been addressed in terms of transcriptomics, microRNA profiling, activation of pro-inflammatory signalling cascades or chromatin-based regulations (reviewed in Pillich, Chakraborty, & Mraheil, 2015). To our knowledge, the effect of *Lm* infection on translation has neither been quantified by mapping the translatome of infected cells, nor by assessing overall changes in protein synthesis rates. As described for other bacterial infections, cap-dependent translation initiation is nonetheless predicted to be transiently impaired during the first hour of infection. Indeed, infection-related stress, and principally membrane pores generated by a secreted perforin, listeriolysin O (LLO), were reported to activate transiently the eIF2α-kinases of the integrated stress response (ISR) pathway and inhibit mTOR signalling, both of which control cap-dependent translation initiation (Gonzalez *et al*., 2011; Shrestha *et al*., 2012; Tattoli *et al*., 2013). Meanwhile, other *Lm* effectors can restore mTOR signalling; for instance the internalisation protein InlB, by binding the cellular receptor Met, is a potent agonist of growth factors signalling cascades, including mTOR (Bhalla, Law, Dowd, & Ireton, 2017). Signalling pathways coordinating overall cellular translation thus receive positive and negative inputs during infection, which are likely to fluctuate over time. On top of these, specific translational regulations may

control the expression of defined subsets of genes, downstream of transcriptional regulation. Ultimately, the possible consequences of modulating host translation on *Lm* infection outcome have not been addressed.

In the present study, we aimed at clarifying the respective contribution of transcriptional and translational regulations on the reshaping of host gene expression of a human epithelial cell line, over a 10-h time course of infection with an epidemic isolate of *Lm*. Using ribosome profiling (Ingolia, Hussmann, & Weissman, 2018), we mapped with high resolution the host translatome during infection, compared it with transcriptome data, and grouped genes that were under transcriptional and/or translational control according to their regulation profiles with regards to time. Our results revealed a dominant pattern, where the rapid induction of gene expression was mainly driven by transcriptional regulation and affected inflammation-related genes, whereas most repressive events were translational, and affected genes encoding components of the translation machinery. The most repressed gene was *PABPC1*, encoding the host cytoplasmic poly(A)-binding protein. Interestingly, preventing *PABPC1* expression by using siRNA-mediated silencing dampened the replication of *Lm*, suggesting that limiting the expression of genes involved in the translational machinery could be part of the cellular responses that help cope with the severity of infection.

Results

Listeria infection does not significantly impair the translation capacity of epithelial cells during the first ten hours of infection

In contrast to what has been shown for other pathogenic bacterial species (Lemaitre & Girardin, 2013), whether infection by *Lm* affects the overall translation activity of host cells was unknown. To assess this, we quantified the ability of a human epithelial cell line from a colon adenocarcinoma (LoVo) to incorporate the methionine analogue homopropargylglycine (HPG) into newly synthesised proteins, over a ten-hour time course of infection by a strain of *Lm* from an epidemic isolate, LL195 (Maury *et al*., 2016; Weinmaier *et al*., 2013) (*Figure 1A*). Infection conditions with this hypervirulent strain were optimised in order to maximize the proportion of infected and viable cells over the period considered. When using a multiplicity of infection (MOI) of 30, bacterial intracellular growth was exponential until 10 h post-infection (p.i.), and the loss of viability of host cells was minimal (*Figure 1—figure supplement 1A*). More than 40% of cells were infected as soon as 2 h p.i. and then, due to cell-to-cell spread of bacteria, the infection expanded so that more than 90% of cells were infected at 5 h p.i (*Figure 1—figure supplement 1B*), which can be considered sufficiently homogeneous for analysing translational effects on cell populations. To avoid possible side effects on host translation due to the change of medium composition in nutrients and growth factors, all experiments were performed using “conditioned medium”, in which cells had been grown for one day before it was pooled and saved.

To evaluate the efficiency of protein synthesis, HPG was added to uninfected or infected cell cultures, one hour prior to each recovery time point, then the labelling of newly-synthesized proteins was revealed by

cycloaddition of HPG residues with sulfo-Cy5-azide, followed by SDS-PAGE and in-gel fluorescent detection (*Figure 1B*). Compared to non-infected cells, no major difference was observed in the overall intensity of HPG incorporation in infected cells at 2, 5 or 10 hours p.i. Whereas total amounts of newly synthesized proteins appeared grossly unchanged, at 10 h p.i., the pattern of labelled proteins started differing, essentially due to the accumulation of an abundant, newly-synthesised protein of ~100 kDa. As expected, treatment of one of the samples with cycloheximide (an inhibitor of translation elongation) concomitantly with HPG addition blocked HPG incorporation, arguing that the detected signals were representative of the cellular activity of protein synthesis.

Lm LL195 thus does not seem to impose a noticeable translational shutoff on its host, but tends on the contrary to maintain a level of protein synthesis comparable to that of uninfected cells. Based on this result, we considered that a translatome analysis of the infected cells could be undertaken, without running the risk that normalizing sequencing data to library size would mask overall changes of translation rates.

Early host gene expression response is dominated by transcriptional activation, while repression events are mainly translational

To clarify whether specific host transcripts were the object of translational regulation during infection, we assessed mRNA expression and translation using high throughput Illumina mRNA sequencing (hereafter, RNA-seq) and ribosome profiling (hereafter, Ribo-seq) from biological samples in triplicates that were either non-infected, or recovered at 2, 5 or 10 h p.i. As expected from this technique, RNA-seq generally had a higher amount of uniquely mapped reads (24 to 32 million) than the Ribo-seq (*Figure 2—figure supplement 1A*). Almost all Ribo-seq samples had nearly 10 million reads or more, except one at the 10 h time-point, which not only had less than three million reads, but also had a smaller proportion of reads mapping to coding sequences (CDS). Consequently, this sample was considered of poor quality and subsequently removed from downstream analysis. Sequenced ribosomal footprints (RFPs) displayed the expected length profile, which peaked at 29 nucleotides (*Figure 2—figure supplement 1B*), typical of high quality Ribo-seq data sets. As expected from Ribo-Seq data, RFPs also mapped predominantly to the coding sequences (CDSs) and 5'-untranslating regions (UTRs), with little mapping to the 3'-UTRs (*Figure 2—figure supplement 1C*). Moreover, mapped RFPs displayed the three-nucleotide codon periodicity characteristic of translating ribosomes (*Figure 2—figure supplement 1D-E*). Infection appeared to have no drastic effect on average translation elongation profiles (*Figure 2—figure supplement 1D*), thus confirming the conclusions drawn from HPG labelling experiments, that overall translation activity is barely perturbed by a 10-h *Lm* infection in epithelial cells.

DESeq2 was used to compute the fold changes in abundance of transcripts between each time point, either in the RNA-seq or in the Ribo-seq datasets. The Spearman correlation coefficients between $\log_2$ fold changes (FC) among differentially regulated genes (DRGs) in the RFP *vs* RNA values were 0.906, 0.771 and 0.759 at [2 *vs* 0], [5 *vs* 2], and [10 *vs* 5] h p.i respectively. The corresponding scatter plots are represented as

Figure 2A-C.

Comparing the 2-hour infected time-point with the non-infected controls, DESeq2 differential expression analysis detected 68 DRGs in the RNA-seq and/or Ribo-seq datasets ($p_{adj} < 0.05$) (*Figure 2A*). Most of these genes clustered next to the diagonal in the upper right quadrant of a Ribo-Seq *vs* RNA-seq scatter plot, highlighting that the dominant feature of gene expression changes during the first two hours of infection is the transcriptional induction of a subset of host transcripts, which then undergo translation without further translational control. Indeed, out of 29 genes displaying a similar differential regulation at the levels of RNA and RFP, all but one were upregulated, with fold changes ranging from 1.7 to 70. *TXNIP*, an inhibitor of anti-oxidative pathways, was the only gene to be statistically significantly repressed (FC: -2, p_{adj}: < 0.01).

Between 2 and 5 h p.i., a total of 621 genes showed differential regulation, in either or both of the datasets (*Figure 2B*). 112 (18%) of these DRGs displayed a similar trend in both the RFP and RNA patterns, indicating that their regulation was driven by changes in their RNA synthesis or decay rates. 319 transcripts (58% of DRGs) appeared as only significantly regulated in the translatome dataset.

Between 5 and 10 h p.i., 4,537 genes were further deregulated, among which 1,078 genes (24% were similarly regulated in both RNA and RFP datasets (*Figure 2C*). All types of differential regulations (positive or negative, affecting the transcriptome or the translatome) were identified, arguing that over time various regulatory mechanisms cooperate to best adapt the expression of each host gene to changing conditions. Note that, due to the loss of one of the translatome samples at the 10 h time points, the proportion of transcripts that qualified as significantly regulated for RFPs in this dataset is likely underestimated.

In order to analyse variations in the translation of each transcript independently of transcript abundance, we then used Riborex to compute changes in translation efficiency (TE) during the course of *Lm* infection. *Figure 2D-F* displays the volcano plots of changes in RNA counts, RFP counts or TE values, between 2 and 5 h p.i. Regarding RNA-seq data, most of the significant DRGs were upregulated (*Figure 2D*, *right*). Nearly all of these were also positively regulated in the RFP data (*Figure 2E*, *right*), corresponding to the genes that grouped next to the diagonal in the upper right quadrant on *Figure 2B*, and for which translation correlated with the transcript abundance. In contrast, a sensibly higher number of genes appeared negatively regulated in the RFP dataset (*Figure 2E*, *left*) than in the RNA dataset (*Figure 2D*, *left*), indicative of the occurrence of repressive events at the translational level. These repressive translational events are more clearly illustrated on *Figure 2F*, where the vast majority of genes that were affected in TE grouped in the left part of the volcano plot. Altogether, this analysis confirm that, while the positive regulation of host gene expression in the first five hours of infection is mainly driven by changes affecting the transcriptome, a subset of genes is affected by translational repression, which is sharply detected between 2 and 5 hours p.i.

Transcriptional induction and translational repression affect functionally distinct biological processes

We then sought to investigate whether genes that were subject to similar changes in their gene expression

also shared functions that might prove relevant to the infectious process. To this end, we performed over-representation analysis (ORA) of gene ontology (GO) biological processes among DRGs which were either up- or down-regulated in RNA-seq, Ribo-seq or TE at each time point of the infection, compared to the non-infected condition (*Figure 3*). The early transcriptional activation highlighted in *Figure 2* led to a pronounced induction of genes associated with pro-inflammatory and type I interferon responses to bacterial invasion (*Figure 3*, first seven lines). As expected, this transcriptional activation was directly mirrored by translation and persisted through to the 5-h time point, when activation of genes related to autophagy, apoptosis and ER stress additionally occurred. At 10 h p.i., the up-or down-regulation of other pathways started emerging, including protein catabolic response, chromatin silencing and mitochondrial metabolism.

The rapid transcriptional induction of pro-inflammatory cytokine and type I interferon genes in response to *Lm* infection has been largely documented (Stavru, Archambaud, & Cossart, 2011). The sensing of pathogen-associated molecular patterns (PAMPs) by cell sensor is known to activate the transcription factor role of NF- κB. Using RcisTarget, we analysed the enrichment for transcription factor binding sites in the promoter regions of the genes that were significantly transcriptionally induced at 2 h p.i. Unsurprisingly, binding sites for NF-κB subunits NFKB1/NFKB2/RELA dominated, with normalized enrichment scores (NES) above 9 confirming that the early induction of NF-κB-dependent signalling during *Lm* infection of epithelial cells drives the inflammatory response. The effects of this early transcriptional activation (followed by a rapid downregulation) on the RNA and RFP profiles of a subset of cytokine genes is illustrated in *Figure 3—figure supplement 1A-B*. At later time points, the weight of NF-κB-dependent transcription declined and the action of additional transcription actors appeared. Between 5 and 10 h p.i., the most enriched motifs upstream of transcriptionally induced genes were binding sites for the stress-responsive transcriptional factors ATF2, ATF3 and ATF6 (NES above 4), highlighting a large contribution of the ISR to the host transcription as infection proceeded. In line with this, the expression of these three transcription factors increased over time (*Figure 3—figure supplement 1C-D*). Altogether, our data confirm an early transcriptional induction of inflammatory pathways in response to infection, which we find to be followed by the activation of the ISR.

Downregulation of functional pathways only emerged between 2 and 5 h p.i. and was largely dominated by translational repression, noticeable in the comparison of Ribo-seq data, and even more obviously when analysing changes in TE. Strikingly, the majority of the transcripts affected by translational repression encoded proteins involved in translation itself (*Figure 3*, lines 14-17). At 10 h post infection, transcripts encoding translation components were further downregulated translationally, while there was also a decrease in the TE of genes regulating the type I interferon response, autophagy and NADH regeneration. As for genes involved in translational regulation, the decrease in TE of genes involved in NADH regeneration was mostly regulated by a decrease in RFPs indicative of repressive translational mechanisms, whereas the decreased TE of genes involved in autophagy and in the regulation of the type I interferon response mirrored differential variations in transcript abundance and translation.

Genes that are translationally co-regulated over time group into functionally-related clusters

To investigate the effect of time on host translation during *Lm* infection, we conducted fuzzy clustering on genes displaying a differential TE in the Riborex analysis, using a cut-off of 0.1 for the adjusted *p* value (p_{adj}). Eight core clusters were generated, representing the major temporal patterns of TE changes during *Lm* infection (*Figure 4A*). Four of these cores (A to D) contained 393 genes that showed an overall increase in TE over the ten-hour time course, while the remaining four cores (E to H) contained 525 genes that displayed an overall decreased TE. In order to assess the functional relevance of these patterns of TE changes, we conducted ORA analysis of GO biological processes on each one of the cluster cores. Six of the cores were statistically enriched for specific GO biological processes.

Transcripts belonging to core B displayed a steady increase in TE throughout the infection and encoded factors involved in distinct biological processes. These included regulation of silencing, either chromatin-based or post-transcriptional, but also genes involved in host response to pathogens, such as type I interferon response, or cellular respiration. Core C was marked by an increase in TE starting after 2 h p.i., and was enriched for genes involved in non-coding RNA metabolism, and predominantly "tRNA metabolic processes".

Core E, in which transcripts were affected by a steady decrease in TE throughout the infection, was enriched for "histone modification" processes and to a lesser extent, "antigen processing and presentation of exogenous antigen" processes, which mostly represent proteins involved in cargo targeting to vesicles and their processing. In Core F, transcripts were affected by a mild decrease in TE that intensified between 5 and 10 h p.i. It was moderately enriched for processes representing "nucleosome disassembly" and "regulation of GTPase activity". All the genes belonging to the "nucleosome disassembly" process encoded proteins participating in transcriptional regulation via chromatin remodelling. Among them, SMARCA4 had been previously reported to exert a repressive role on E-cadherin transcription (Sánchez-Tilló *et al*., 2010). Genes belonging to the "regulation of GTPase activity" process mainly encoded regulators of actin dynamics or vesicle formation and processing. Altogether cores E and F, both of which present a temporal decrease in TE, are broadly enriched for genes involved in chromatin-based regulation, vesicle formation and processing.

Cores G and H were characterized by a slight increase in TE at 2 h p.i. followed by a prominent decrease between 2 and 5 h p.i., which was further amplified until 10 h in core G whereas it plateaued after 5 h in core H. In both of these clusters, changes in TE were largely due to a strong decrease in the abundance of RFPs (rather than by an increased in RNA-seq), suggesting these genes were actually translationally repressed rather than buffered by a lack of translation. Core G was moderately enriched for genes related to the "regulation of canonical glycolysis". In contrast, core H contained essentially genes encoding factors involved in ribosome biogenesis and protein synthesis; indeed, 80% of them encoded ribosomal proteins, translation initiation or elongation factors. A few additional genes were associated with related biological processes, such as "mRNA catabolism", "protein stability", and "autophagy".

In terms of number of co-regulated genes, the enrichment of core H with factors required for host translation was the most striking feature of the fuzzy clustering and ORA analysis. We then asked whether specific features within these functionally-related transcripts could determine their co-regulation.

5'-terminal oligopyrimidine motif-containing mRNAs are co-repressed translationally during *Listeria* infection

Several *cis*-acting motifs within the sequence of mRNAs have previously been described for their ability to modulate eukaryotic translation initiation in response to cellular stresses or infection. Among them, four classes of motifs located in the 5'-UTRs of transcripts can have a significant influence on the efficiency of recruitment of the translation pre-initiation complex (PIC) or of initiation at the appropriate AUG, namely: translation initiator of short 5′UTRs (TISU), 5'-terminal oligopyrimidine motifs (5'-TOP), internal ribosome entry site (IRES) structures, or upstream open reading frames (uORF) (reviewed in Hinnebusch, Ivanov, & Sonenberg, 2016). To assess whether the presence of these motifs could dictate the co-regulation of the transcripts that were translationally repressed during infection, we tested whether the repressed gene set displayed a statistically significant enrichment for any of these motifs using ROAST. Out of the 1,003 genes that had differential TE across any one condition as calculated by Riborex, 82 were only translationally regulated and had more than two fold change in RFP levels with stable transcript abundance across the ten-hour time-course. We found that there was a significant enrichment of TOP genes at 10 h p.i. (ROAST p_{adj} = 0.021), whereas none of the other motifs were statistically enriched.

To further illustrate this enrichment, we displayed the distribution of changes in TEs during infection for each list of experimentally validated TOP- (n = 83), uORF- (n = 76) or IRES- (n = 25) containing transcripts, or for the 133 transcripts containing a TISU motif with no mismatch (*Figure 5A-D*). After a modest increase in TE for the bulk of TOP-containing transcripts at 2 h p.i., they consistently displayed a decrease in TE at 5 h p.i., which exacerbated at 10 h p.i. (*Figure 5A*). In contrast, the distributions of uORF-, IRES- or TISU-containing transcripts remained centred on 0 (*Figure 5B-C*). The individual profiles for each one of the transcripts belonging to each category revealed individual variability within the general trends (*Figure 5E-H*), and emphasised a high similarity in profiles between TOP-containing transcripts (*Figure 5E*) and core cluster H (*Figure 4A*). Interestingly, the only two transcripts that displayed a decrease in TE as soon as 2 h p.i. were *PABCP1* and *PABPC4* with *PABPC1* being the most heavily repressed of all TOP-containing transcripts (*Figure 5E*).

PABPC1 is translationally repressed during *Listeria* infection of epithelial cells

PABPC1 and *PABPC4* encode cytoplasmic poly(A)-binding proteins (PABP), and are the only two members of this family to be expressed in LoVo cells. Both transcripts undergo a potent translational inhibition, which deepens as the infection proceeds even though their transcript abundance increased slightly over time (*Figures 5E and 6A-C*). Because *PABPC1* was the most expressed of the two paralogues and

displayed the most striking repression, we focussed on the regulation of the expression of this gene during *Lm* infection. Using fluorescence *in-situ* hybridization (FISH) against *PABPC1* mRNA, we confirmed that its abundance did not decline in infected cells, even though a noticeable heterogeneity between individual cells could be noticed at all time points (*Figure 6—figure supplement 1*). The cytoplasmic location of *PABPC1* transcripts was generally diffuse, and a small proportion of the signal co-localised with the P-body marker DDX6. No remarkable change in the proportion of *PABPC1* mRNA localising to P-bodies was observed throughout the infection time-course, arguing that sequestration of the transcript within these compartments could likely not account for the intensity of the translational repression detected in our analysis.

De-regulation of *PABPC1* expression impacts on *Listeria* intracellular replication

The potent control exerted on *PABPC* mRNA translation prompted us to scrutinize if cytoplasmic PABPC1 translation or abundance was having an impact on infection progression. Indeed, in a previously published siRNA screen for host factors involved in *Lm* infection of HeLa cells, silencing of *PABPC3* (which is not expressed in LoVo cells), and to a lesser extent *PABPC1*, was shown to reduce intracellular bacterial loads measured at 5 h p.i. (Kühbacher *et al*., 2015). We hypothesised that reducing the synthesis of PABPCs during infection might facilitate the ability of infected cells to control bacterial intracellular multiplication. To test this hypothesis, we transfected LoVo cells with siRNA against *PABPC1*, or with a control scrambled siRNA, 48 h before infecting with *Lm*, and then monitored the intracellular replication of bacteria in cells (*Figure 6D*). Colony forming units (CFU) counts were normalized to values measured at 2 h p.i. in order to analyse only the intracellular multiplication of bacteria rather than possible variations in entry into cells. When *PABPC1* was silenced in LoVo cells, we observed a reduced intracellular replication rate, compared to cells transfected with the control siRNA (*Figure 6D*). These observations suggest that repressing the expression of cytoplasmic PABPs could participate in cellular control of bacterial proliferation.

Discussion

Regulation of gene expression allows organisms to respond to changes in their environment. The intensity and kinetics of the response is strongly influenced by the nature of the regulatory mechanisms involved, affecting various levels on the path from DNA to end-products. In the present study, we aimed at clarifying the respective contribution of transcriptional and translational regulations on the reshaping of host gene expression of a human epithelial cell line, over a 10-h time course of infection with an epidemic isolate of *Lm*. Metabolic labelling with homopropargylglycine revealed that *Lm* infection did not drastically impair the overall translation capacity of infected epithelial cells. By comparing translatome with transcriptome data, we then identified genes that were under transcriptional and/or translational control, and grouped them according to their regulation profiles with regards to time. Our results revealed a dominant pattern, where the rapid induction of gene expression was mainly driven by transcriptional regulation, whereas most repressive

events were translational. Over-representation analysis of gene ontologies also highlighted a frequent co-regulation of genes encoding proteins involved in related biological processes. Typically, whereas inflammation was transcriptionally induced, most genes encoding components of the translation machinery were translationally repressed, likely due to a strong repression of the translation of mRNAs harbouring a 5'-terminal oligopyrimidine (TOP) motif. The most repressed gene was *PABPC1*, encoding the main host cytoplasmic PABP. Interestingly, further repressing *PABPC1* expression using siRNA-mediated silencing dampened the replication of *Lm*, suggesting that limiting the expression of the translational machinery could be part of the cellular responses that helps the cell cope with the severity of infection.

Contribution of infection-induced stress response to gene expression regulation

In addition to the expected early activation of NF- κB and its pro-inflammatory effect, a large part of the regulations we uncovered could be explained by the inhibition of mTOR signalling and the activation of the ISR. Indeed, the induction of ISR and repression of mTOR signalling in response to *Lm* infection was previously described (Shrestha *et al*., 2012; Tattoli *et al*., 2013), and was mainly dependent on the pore-forming activity of LLO (Tattoli *et al*., 2013). Treatment of RPE1 cells by LLO was also shown to trigger a transient phosphorylation of eIF2α—a hallmark of ISR—, as well as a transient arrest in total protein synthesis (Gonzalez *et al*., 2011). However, our results appear to differ significantly from the existing literature, both in terms of kinetics and intensity. First, no transient arrest in overall protein synthesis occurred during the course of our 10-h infection of LoVo cells (*Figure 1*), suggesting that the drastic effects on protein synthesis observed when cells were treated with an elevated dose of LLO (0.5 or 1 μg/mL, *i.e*. 9 to 18 nM) was not representative of the real exposure of cell membranes to the toxin when it is secreted by invading bacteria. Second, translational and transcriptional effects that could be attributed to the induction of the ISR appeared gradually over time, and became noticeable in transcriptome data only after 10 h of infection (*Figure 3—figure supplement 1*). The translation of *ATF4*, which is known to be induced upon phosphorylation of eIF2α due to the presence of a series of uORFs in its 5'-UTR, only modestly increased during infection. The transcription and translation of ATF3 increased gradually over time from the beginning of infection, while the induction of ATF6 only occurred between 5 and 10 h p.i. In line with this, the transcriptional targets of ATF3 and 6 were upregulated at 10 h p.i. These observations suggest that the transcriptional effects of the ISR induced by *Lm* infection could be more gradual and long-lasting than what was suggested by previous measurements of transient eIF2α phosphorylation (Shrestha *et al*., 2012; Tattoli *et al*., 2013). Part of this discrepancy may have arisen from noticeable differences between our experimental setup and that of others. For instance, we used a lower multiplicity of infection (30 rather than 100) and lower centrifugation speed (1.5 min at 200 × *g* rather than 1 min at 2,000 × *g*) than Talloli *et al*., which could reduce mechanical stress on cells in the first steps of infection. We have also used conditioned medium throughout our experiments to avoid any possible effects on the sensing of amino-acid starvation when replacing media. Altogether, we hypothesize that our milder conditions of cell culture and infection were

responsible for delaying and lengthening the effects of the ISR activation reported by others.

Another important difference between our experimental conditions and that of others was the use of an epidemiological isolate of *Lm*, the biology of and host response to which have scarcely been addressed to date. The selected strain LL195 belongs to the clonal complex 1 within lineage I of *Lm* (Maury *et al*., 2016), which is more representative of clinical cases of listeriosis than usual laboratory strains such as EGD-e or 10403S belonging to *Lm* lineage II. The haemolytic titre we measured for LL195 did not differ significantly from that of EGD-e, arguing against a lack of LLO activity in this strain. However, we cannot exclude that the different repertoire of virulence factors expressed by this strain might impact the host cell response and possibly dampen ISR, compared with reference strains.

In addition to the gradual induction of ISR, our work highlights a strong translational repression of TOP-containing transcripts starting between 2 and 5 h p.i., perhaps resulting from repression of the mTOR signalling pathway. The current model for the translational co-regulation of TOP mRNAs involves the direct binding of LARP1, a target of mTOR kinase activity, to TOP motifs (Fonseca *et al*., 2015). When mTOR is inhibited, LARP1 becomes dephosphorylated and strongly binds TOP motifs, preventing mRNA translation initiation. Given the previously-documented inhibition of mTOR activity in response to *Lm* infection (Tattoli *et al*., 2013), our data is consistent with this inhibition leading to the recruitment of LARP1 on TOP motifs, and to the potent downregulation of the transcripts harbouring them.

It was also recently found that during exposure to sodium arsenite —a potent stress inducer that results in mTOR inhibition—, LARP1 was responsible for the recruitment of a fraction (10-15%) of TOP mRNAs to stress granules and P-bodies (Wilbertz *et al*., 2019). Whereas we could detect a small proportion of the TOP-containing mRNA *PABPC1* in association with P-bodies (*Figure 5—figure supplement 1*), in our experimental conditions (LoVo cells grown in conditioned medium), this proportion did not vary throughout the infection time-course, arguing against the docking of *PABPC1* to P-bodies being required for its translational repression.

Dynamics of gene expression response to *Listeria* infection

An important parameter addressed by our study is the timing of the host response to infection, and how different layers of gene expression control contribute to this timing. By studying a time-course of infection rather than a unique time point as had been done in most studies to date, and by quantifying not only the transcriptome but also the translatome, we reveal that in the first hours of infection most activation events are transcriptional, whereas most repression events are translational. This rather binary effect is easily understandable by taking mRNA steady-state levels and turnover into account. Before infection, virtually no mRNA encoding cytokine genes is present in cells; therefore their induction necessarily requires, first transcription, and then translation. In contrast, mRNAs encoding components of the translation machinery are highly abundant. In addition, the intrinsic stability of human mRNAs is relatively high compared with the kinetics of an infection. Estimates of the median half-lives of mRNAs in mammalian cells are in the range of

hours; among these, the half-lives of transcripts from housekeeping genes, especially those encoding translation factors and ribosomal proteins, are among the longest and often above 10 h (Schwanhäusser *et al*., 2011; Tani *et al*., 2012). As a consequence, downregulating the quantity of these transcripts by merely tuning down their transcription would take days. The most effective ways for a cell to rapidly stop the synthesis of proteins from this pathway would thus be either to massively degrade transcripts or to inhibit their translation. The second process —which we found to be prevalent between 2 and 5 h p.i.— is reversible; this might constitute an advantage during recovery from stress by allowing a rapid resumption of the translation of the previously-repressed genes. In the longer term, other types of regulation may take place; for instance, the downregulation of cytokine gene expression after 2 h p.i. likely relies both on the reduction of their transcription, and on the generally short half-life for this class of transcripts (Tani *et al*., 2012). Moreover, in addition to these broad rules drawn from the dominating patterns we observed, a number of individual transcripts are likely finely tuned by a combination of actions on transcription, decay and translation.

One level of regulation that was not addressed in our work was protein stability, which also should consistently contribute to the timing and effectiveness of the regulations we observed. Drastic alterations in the cell proteome and protein turnover in response to *Lm* infection or to treatment with LLO have previously been described (Malet *et al*., 2018; Ribet *et al*., 2010), and it would be interesting to integrate host proteomic data over an infection time course to assess how translation and proteome degradation contribute to reshaping the cell equipment. By western blot, we have verified that the total amounts of PABPC1 and several ribosomal proteins were not affected during the course of our experiment, probably due to their long half-lives (data not shown). In case the reduction of the amount of these proteins is playing a role by controlling the overall translation capacity of cells, it must thus be considered in a longer course of infection. In agreement with this, we did not monitor any reduction in total protein synthesis activity within the 10 h we examined.

An alternative hypothesis would be that a reduction of the translation of TOP-containing mRNAs might impact infection outcome, rather than the reduction of the amounts of its products. One could for instance imagine that, by pausing their anabolic metabolism and saving on the synthesis of abundant translation components, cells facing a bacterial challenge could reallocate part of their resources to antibacterial defences. Testing these hypothesis will deserve future investigations.

Effects of the repression of *PABPC1* expression on bacterial or viral infections

Among the TOP-containing transcripts, *PABPC1* was the one most translationally repressed. The fact that pre-silencing its expression before infection reduces the intracellular multiplication rate of *Lm* suggests that the host cell can benefit from dampening its expression. As discussed above for the bulk of TOP genes, this could either be due to a saving of resources by the host cell when avoiding the synthesis of a very abundant protein, or to a possible contribution of PABPC1 protein in the host bacterial dialogue. To the best of our knowledge, no direct role for PABPs in the response to a bacterial infection has been documented.

And yet, a few pieces of evidence indicate that PABPs could contribute to the regulation of inflammation and innate immune responses. For instance, blocking the ability of PABPs to bind poly(A) tails has been shown to reduce the sensitisation of mice to pain by blocking protein synthesis and neurogenic inflammation in response to pro-inflammatory signals (Barragán-Iglesias *et al*., 2018). More relevant to host pathogen interactions, the product of an interferon-stimulated gene, RyDEN, was shown to restrict the replication of a variety of viruses by forming an inhibitory complex with PABPC1 and LARP1 (Suzuki *et al*., 2016). Both PABPC1 and LARP1 were positive regulators of Dengue virus (DENV) replication, reminiscent of our present findings for *Lm* intracellular multiplication. RyDEN was then hypothesized to interfere with DENV translation, which could not hold true in the case of a bacterial pathogen. A possible explanation to both phenotypes seen for *Lm* and DENV infections, and that would need testing, might be that PABPC1 inhibition would favour the expression of innate immune effectors that might help counteract infections.

Conclusions

In response to *Lm* infection, the downregulation of host translation seemed to affect only a specific subset of transcripts: 5'-TOP-containing mRNAs. Given that the translational regulation of this class of transcripts is known to be driven by the mTOR/LARP1 pathway (Fonseca *et al*., 2015), it is reasonable to speculate that the coordinated repression of transcripts encoding the cell translation equipment would represent a host response to infection, rather than a bacterial strategy to subvert cell function. This contrasts with the translational repression observed during *Lp* infection (Barry *et al*., 2017), which consistently affected the whole translatome of infected cells, and depended on the inhibitory function of at least four secreted *Lp* effectors on host translation elongation (Fontana *et al*., 2011). Whether *Lm* effectors that might likewise interfere with host translation also exist in *Lm* remains an open question.

Material and methods

Bacterial strains and culture conditions

The bacterial source strains used for this work were *Escherichia coli* NEB5α (New England BioLabs) for plasmid constructions, and *Listeria monocytogenes* LL195 (Weinmaier *et al*., 2013) for all of the experiments involving *Lm*. All strains were grown at 37°C under shaking at 190 rpm in Luria Bertani (LB) medium for *E. coli*, in brain hear infusion (BHI) for *Lm*. Whenever required, media were supplemented with antibiotics for plasmid selection (chloramphenicol, 35 µg/mL for *E. coli*; 7 µg/mL for *Lm*).

Culture, infection and transfection of epithelial cells

Infections were performed in LoVo cells, an intestinal epithelial cell line originating from a colon adenocarcinoma (ATCC® CCL-229™, Manassas, VA, USA). Cells were maintained in F-12K Nut Mix media (Thermo Fischer Scientific, FR), supplemented with 10% heat inactivated fetal bovine serum (PAN Biotech, FR) at 37°C and 5% CO_2. Cells were passage 14 before seeding and were grown to 70-85% confluence prior

to infection. The cell culture medium was changed every 24-h and kept for further use during the infection as "conditioned medium". When needed, cells were transfected 48 h before infection with siRNA using RNAiMAX in 24 well format as per manufacturer's recommendations. Knockdown of targeted protein was confirmed with western blot.

One colony of *Lm* was grown until they reached stationary phase (OD_{600} of 2 to 3) in BHI media at 37°C. Bacteria were washed with PBS, and add to a cell monolayer in the cell culture flasks (for Hi-seq or HPG incorporation experiments) or in 24-well plate format (for gentamicin protection assay experiments) at ~75-90% confluence. The cell culture flasks or plates were centrifuged at 200 × *g* for 1 minute and then incubated at 37°C and 5% CO_2 for 30 minutes. Cells were then washed with PBS containing 40 µg/µL gentamicin and conditioned media containing 25 µg/mL gentamicin was added. Infection was allowed to proceed until specific time points after which culture plates were snap-frozen in liquid nitrogen and stored at -80°C (for Hi-seq or HPG incorporation experiments) or cells were washed in PBS and trypsinised for counting.

For gentamicin protection assays, cells were counted using a LUNA II automated cell counter and then centrifuged at 700g for 5 minutes. The cell pellet was re-suspended in water, incubated for 5 minute, and then titrated through a 25G needle. Cell lysate was diluted in PBS and plated on BHI agar before overnight incubation at 37°C. Colony forming units were counted and normalized to cell counts to attain CFU/Cell.

Western Blot

Total cell lysate was prepared by adding Laemmli sample buffer supplemented with Pierce™ Universal Nuclease (Thermo Scientific™) and protease inhibitor cocktail directly to the cell monolayer. The monolayer was scrapped and the lysate was transferred to an Eppendorf tube after which samples were heated 95°C for 5 minutes and either stored at -80°C or used directly. Samples were migrated on a 12% SDS-PAGE gel and transferred to PVDF membrane using a Pierce G2 Fast Blotter (Thermo Scientific). Membranes were blocked in 5% w/v milk or BSA, TBS, 0.1% Tween® 20 according to antibody manufacturer's recommendations. Rabbit polyclonal antibodies against PABPC1 (Atlas Antibodies #HPA045423) or mouse monoclonal antibodies against actin were added to the blocking solution at a 1/500 dilution, and incubated overnight at 4°C. Membranes were incubated with corresponding secondary antibody (Bethyl Mouse or Rabbit IgG heavy and light chain antibodies coupled to HRP, # A120-101P and A90-116P) at a 1:50 000 dilution in the same buffer for 2 hours at room temperature. Signal was revealed using Pierce® ECL Western Blotting Substrate on an ImageQuant™ LAS 4000 mini.

Global translation using HPG incorporation and fluorescent labeling by copper catalyzed cycloaddition

Lovo cells were grown to 70-85% confluency in T75cm^2 flasks and infected with *Lm* as described above. L-Homopropargylglycine (HPG, Jena Biosciences #CLK-016) was added at 2 mM final concentration 1 hour prior to each experiment end-point. Cells were snap frozen in liquid nitrogen and stored at -80°C. For

copper-catalyzed alkyne-azide cycloaddition (click reaction), cells were lysed with click reaction compatible lysis buffer (100 mM HEPES, 150 mM NaCl, 1% Igepal-CA 630) after which a click reaction was performed with Sulfo-Cy5-Azide (Jena Bioscience) at the following concentrations: 1 µg/µL protein, 100 µM azide sulfo Cy5 or azide-biotin, 1 mM Cu(II) sulfate, 5 mM Tris(3-hydroxypropyltriazolylmethyl)amine (THPTA), and 1 mM sodium ascorbate. Cu(II) sulfate was mixed with the THPTA prior to addition to the click reaction. Components were always added in the following order: azide-conjugate, Cu(II) sulfate-THPTA complex, and sodium ascorbate. The click reaction was allowed to proceed for one hour at room temperature. Samples were then methanol/chloroform precipitated and resuspended in Laemmli sample buffer. Samples were denatured at 95°C for 5 minutes and separated on a 12% SDS-PAGE gel. The gel was scanned with a Typhoon FLA 7000 biomolecular imager after which it was stained with colloidal Coomassie Brillant blue G-250 as previously described (Neuhoff, Arold, Taube, & Ehrhardt, 1988). Cycloheximide treated or no-treatment cells were used as negative controls.

Importantly, the cells were not starved of methionine prior to addition of HPG so that amino acid metabolism pathways remained unperturbed.

Immunofluorescence and FISH on infected cells

LoVo cells were seeded in 24-well plates containing 12 mm diameter coverslips. Infection with bacteria expressing eGFP was performed as described above. At specified time-points, cells were fixed for 15 minutes with 4% paraformaldehyde/PBS, washed with PBS then stored at 4°C until further processing. Prior to staining, cells were permeabilized for 5 min at room temperature with 0.5% Triton X-100 in PBS. Cells were then blocked for 30 min in PBS buffer containing 2 % bovine serum albumin (BSA, Sigma) and incubated with Acti-Stain™ 670 fluorescent phalloidin (Cytoskeleton #PHDG1, 70 nM) and DAPI (0.1 µg/µl) for one hour. After three additional washes, cover glasses were mounted on microscope slides with Fluoromount mounting medium (Interchim). For PABPC1 FISH, a set of 48 Stellaris RNA FISH probes (Quasar ® 670 dye) against PABPC1 were designed using the Stellaris Probe Designer. PABCP1 mRNA FISH and immunofluorescent co-staining was done according to the Stellaris ® RNA FISH protocol. Antibodies and counter-stain used included DDX6 primary antibody (Bethyl; A300-460A; 1:500; Rabbit), Cy3-goat-anti-rabbit secondary antibody (Jackson ImmuneResearch; 1:500), l), and 4', 6-diamidino-2-phenylindole (5 ng/mL DAPI).

Preparations were observed with a Nikon Ti epifluorescence microscope (Nikon), connected to a digital CMOS camera (Orca Flash 4.0, Hamamatsu). Illumination was achieved using a SOLA-SE 365 source (Lumencor) and the following excitation/emission/dichroic filter sets (Semrock): DAPI, 377(50)/447(60)/FF409-Di03 ; Acti-Stain 670 or eGFP, 472(30)/520(35)/FF495-Di03. Images were acquired with Nikon apochromat 60x objective lenses (NA 1.4) and processed with the MicroManager and Fiji software. Each image is representative of the infected cell population.

RNA-seq and Ribo-seq sample preparation

Lovo cells were grown to 70-85% confluency in T75cm^2 flasks and infected with *Lm* LL195 as described above. Flasks were snap frozen in liquid nitrogen before infection (0 h) and at 2, 5, and 10 hours p.i., and then stored at -80C° until further use. Ribosome footprinting was done as per the protocol of Ingolia *et al*. Briefly, lysis buffer (20mM Tris pH 7.4, 150 mM NaCl, 5 mM MgCl, 1% TritonX, 1 mM DTT, 25 U/mL TurboDNase) was added to the frozen monolayer, which was then scrapped and transferred to an Eppendorf tube and processed. A portion of the lysate was taken, and acid phenol was used to extract total mRNA, which was stored at -80°. Ribosome footprinting was performe on the same biological sample by adding RNAseI to the lysate at 2.5U/µL for 45 minutes at room temperature. The digestion was stopped by adding SuperaseIN (0.66U/µL) and ribosomes were purified by ultracentrifugation on a 1 M sucrose cushion. Ribosome protected fragments were extracted using acid phenol and used in sequencing library construction. Each time course was reproduced twice at a one week interval, thus producing biological triplicates.

RNA-seq library construction

The IBENS Genomics Facility conducted the RNA-seq library construction. Isolated total cytoplasmic RNA integrity was verified using the RNA Pico method on the Agilent 2100 Bioanalyzer. High-quality RNA (RIN > 8) was used in library preparation for with the Illumina TruSeq stranded protocol (Illumina, San Diego,USA). Libraries were rRNA depleted using the Illumina Ribo Zero kit and sequenced as single read 75 base pair read length (SR75) on the NextSeq 550 system by the IBENS Genomics Facility.

Ribo-seq library construction

Library construction was done using a protocol adapted from Huppertz *et al*. Briefly, RFPs were gel purified on polyacrylamide TBS-urea gels. The RFPs ends were then de-phosphorylated using T4 PNK and the 3'clip primer adaptor was ligated using T4 RNA ligase 2, truncated (New England Biolabs, #M0242). The ligated RFPs were gel purified and the RFPs were converted to cDNA using primers that contained barcodes and randomized nucleotides in order to remove PCR duplicates. The cDNA was then circularized using Circligase II (Lucigen, #CL4111K) and then linearized using BamHI. rRNA purification was performed as previously described (Ingolia, Brar, Rouskin, McGeachy, & Weissman, 2012), with two modifications: (1) extra rRNA oligos were added to the biotinylated oligonucleotide cocktail, and (2) a second bead purification step was added. Purified RFP cDNA was amplified using Solexa primers and the libraries were sequenced as single read 75 base pair read length (SR75) on the NextSeq 550 system by the IBENS Genomics Facility.

The complete lists of oligonucleotides used for library constructions is supplied as Tables S1.

Read processing

RNA-seq reads that passed the Illumina quality filter were aligned to rRNA (pre-rRNA 45S + rRNA 5S

sequences from NCBI Nucleotide Database) using Bowtie2 (v2.3.2). Reads that were not mapped to rRNA were retained and aligned to the human genome (GRCh38) using STAR (v2.5.3a) (Dobin *et al*., 2013). Uniquely mapped reads were counted using featureCounts (v1.5.0) (Liao, Smyth, & Shi, 2014).

For Ribo-seq reads, barcoded files were generated for each multiplexed fastq file. Reads that passed the IQF were then processed to remove PCR duplicates, which were identified by five random bases flanking the sample-specific barcodes. Reads that matched at these five random positions were classified as PCR duplicates and only the first hit was kept for further processing. Reads were trimmed (removing the 5'index and 3'adaptor) using cutadapt (v1.10) with option "-m/--minimum-length 25" to discard reads shorter that 25 nucleotides after adapter trimming. Trimmed reads were aligned to rRNA sequences as described above. The remaining reads were aligned to the human genome (GRCh38) using STAR (option '*--sjdbOverhang 40'*). Uniquely mapped reads were counted using featureCounts (v1.5.0).

All Hi-seq data discussed in this publication have been deposited in the European Nucleotide Archive (Leinonen *et al*., 2010) and are accessible under accession number PRJEB26593 (https://www.ebi.ac.uk/ena/data/view/PRJEB26593).

Data analysis and visualization

Library size normalized read alignments were visualized using the Integrative Genomics Viewer (IGV) from bedgraph files generated using samtools and bedtools. Post-mapping quality control and analysis of the distribution of reads by category of annotated genomic features was performed using ALFA (Bahin *et al*., 2019). Differential expression (RNA-seq) and differential translation (Ribo-seq) data were analyzed using DESeq2 (Love, Huber, & Anders, 2014). Translational efficiency was calculated and differential TE was analyzed using RiboRex with a DESeq2 engine (Li, Wang, Uren, Penalva, & Smith, 2017). Functional enrichment analysis was conducted using over representation analysis of GO biological processes with the clusterProfiler R package (Yu, Wang, Han, & He, 2012) on genes that had a false discovery p-value < 0.05 in the DESeq2 or RiboRex analysis. Enrichment for transcription factor binding sites in the 500 bp region located upstream of the transcription start sites of RNA-seq DRGs was conducted using RcisTarget (Aibar *et al*., 2017), which is R implementation of iRegulon (Janky *et al*., 2014). Fuzzy clustering of TE values was performed using the Mfuzz package (Futschik & Carlisle, 2005). For the fuzzy clustering, TE values were recalculated by dividing TMM normalized (edgeR package) Ribo-seq counts by RNA-seq counts (Robinson & Oshlack, 2010; Robinson, McCarthy, & Smyth, 2010). Only those genes that had an FDR p-value < 0.05 as computed by RiboRex at any time-point were included in order to decrease noise during clustering. ROAST (Rotation gene set tests for complex microarray experiments) (Wu *et al*., 2010) was used for gene set testing of TOP-, uORF-, IRES-, or TISU-containing transcripts. The list of transcripts containing TOP motifs (Yamashita *et al*., 2008), uORFs (McGillivray *et al*., 2018) or IRES (Mokrejs *et al*., 2006) had been experimentally verified. In contrast, the list of transcripts containing a TISU motif with no mismatch was computed (Sinvani *et al*., 2015).

Acknowledgements

We warmly thank Zhen Wang for sharing with us her optimized Ribo-Seq protocol, and invaluable advice about how to best handle this technique. We are grateful to Caroline Peron Cane, Cholé Connan and José-Carlos Fernandez for their precious experimental assistance and eagerness to help solve technical issues. Last we thank the IBENS genomics platform for their careful sequencing of all samples, patient assistance and dedication, as well as the Computational Biology Centre for maintaining access to the servers, and Imaging facility for maintaining access to microscopy equipment.

Author contributions

AL designed the project. VB and AL devised experiments and interpreted results. VB performed experiments with the help of SR for *Lm* genetics, FISH and immunofluorescence. FH, BN and VB analysed High-Seq data under supervision by AG and AL. VB and AL designed graphics and wrote the manuscript.

Funding

Work in the group of AL has received support under the program "Investissements d'Avenir" implemented by ANR (ANR-10-LABX-54 MemoLife and ANR-10-IDEX-0001-02 PSL University), Fondation pour la Recherche Médicale (FRM-AJE20131128944), Inserm ATIP-Avenir and Mairie de Paris (Programme Émergences – Recherche médicale). SR benefitted from SNF Early Postdoc Mobility grant P2BEP3_168721.

Declaration of interests

The authors declare that they have no competing interests.

References

Aguilar, C., Mano, M., & Eulalio, A. (2019). MicroRNAs at the Host-Bacteria Interface: Host Defense or Bacterial Offense. *Trends in Microbiology*, *27*(3), 206–218. http://doi.org/10.1016/j.tim.2018.10.011

Aibar, S., González-Blas, C. B., Moerman, T., Huynh-Thu, V. A., Imrichova, H., Hulselmans, G., *et al.* (2017). SCENIC: single-cell regulatory network inference and clustering. *Nature Methods*, *14*(11), 1083–1086. http://doi.org/10.1038/nmeth.4463

Bahin, M., Noël, B. F., Murigneux, V., Bernard, C., Bastianelli, L., Le Hir, H., *et al.* (2019). ALFA: annotation landscape for aligned reads. *BMC Genomics*, *20*(1), 250. http://doi.org/10.1186/s12864-019-5624-2

Barragán-Iglesias, P., Lou, T.-F., Bhat, V. D., Megat, S., Burton, M. D., Price, T. J., & Campbell, Z. T. (2018). Inhibition of Poly(A)-binding protein with a synthetic RNA mimic reduces pain sensitization in mice. *Nature Communications*, *9*(1), 10. http://doi.org/10.1038/s41467-017-02449-5

Barry, K. C., Ingolia, N. T., & Vance, R. E. (2017). Global analysis of gene expression reveals mRNA superinduction is required for the inducible immune response to a bacterial pathogen. *eLife*, *6*. http://doi.org/10.7554/eLife.22707

Bhalla, M., Law, D., Dowd, G. C., & Ireton, K. (2017). Host serine/threonine kinases mTOR and protein

kinase C-α promote InlB-mediated entry of *Listeria monocytogenes*. *Infection and Immunity*, *85*(7), e00087–17. http://doi.org/10.1128/IAI.00087-17

Cornejo, E., Schlaermann, P., & Mukherjee, S. (2017). How to rewire the host cell: A home improvement guide for intracellular bacteria. *The Journal of Cell Biology*, *216*(12), 3931–3948. http://doi.org/10.1083/jcb.201701095

Dobin, A., Davis, C. A., Schlesinger, F., Drenkow, J., Zaleski, C., Jha, S., *et al*. (2013). STAR: ultrafast universal RNA-seq aligner. *Bioinformatics*, *29*(1), 15–21. http://doi.org/10.1093/bioinformatics/bts635

Duval, M., Cossart, P., & Lebreton, A. (2017). Mammalian microRNAs and long noncoding RNAs in the host-bacterial pathogen crosstalk. *Seminars in Cell & Developmental Biology*, *65*, 11–19. http://doi.org/10.1016/j.semcdb.2016.06.016

Fonseca, B. D., Zakaria, C., Jia, J.-J., Graber, T. E., Svitkin, Y., Tahmasebi, S., *et al*. (2015). La-related Protein 1 (LARP1) Represses Terminal Oligopyrimidine (TOP) mRNA Translation Downstream of mTOR Complex 1 (mTORC1). *The Journal of Biological Chemistry*, *290*(26), 15996–16020. http://doi.org/10.1074/jbc.M114.621730

Fontana, M. F., Banga, S., Barry, K. C., Shen, X., Tan, Y., Luo, Z.-Q., & Vance, R. E. (2011). Secreted bacterial effectors that inhibit host protein synthesis are critical for induction of the innate immune response to virulent *Legionella pneumophila*. *PLoS Pathogens*, *7*(2), e1001289. http://doi.org/10.1371/journal.ppat.1001289

Futschik, M. E., & Carlisle, B. (2005). Noise-robust soft clustering of gene expression time-course data. *Journal of Bioinformatics and Computational Biology*, *3*(4), 965–988.

Gonzalez, M. R., Bischofberger, M., Frêche, B., Ho, S., Parton, R. G., & van der Goot, F. G. (2011). Pore-forming toxins induce multiple cellular responses promoting survival. *Cellular Microbiology*, *13*(7), 1026–1043. http://doi.org/10.1111/j.1462-5822.2011.01600.x

Hinnebusch, A. G., Ivanov, I. P., & Sonenberg, N. (2016). Translational control by 5'-untranslated regions of eukaryotic mRNAs. *Science (New York, NY)*, *352*(6292), 1413–1416. http://doi.org/10.1126/science.aad9868

Ingolia, N. T., Brar, G. A., Rouskin, S., McGeachy, A. M., & Weissman, J. S. (2012). The ribosome profiling strategy for monitoring translation in vivo by deep sequencing of ribosome-protected mRNA fragments. *Nature Protocols*, *7*(8), 1534–1550. http://doi.org/10.1038/nprot.2012.086

Ingolia, N. T., Ghaemmaghami, S., Newman, J. R. S., & Weissman, J. S. (2009). Genome-wide analysis *in vivo* of translation with nucleotide resolution using ribosome profiling. *Science (New York, NY)*, *324*(5924), 218–223. http://doi.org/10.1126/science.1168978

Ingolia, N. T., Hussmann, J. A., & Weissman, J. S. (2018). Ribosome Profiling: Global Views of Translation. *Cold Spring Harbor Perspectives in Biology*, a032698. http://doi.org/10.1101/cshperspect.a032698

Janky, R., Verfaillie, A., Imrichova, H., Van de Sande, B., Standaert, L., Christiaens, V., *et al*. (2014). iRegulon: from a gene list to a gene regulatory network using large motif and track collections. *PLoS Computational Biology*, *10*(7), e1003731. http://doi.org/10.1371/journal.pcbi.1003731

Kühbacher, A., Emmenlauer, M., Rämo, P., Kafai, N., Dehio, C., Cossart, P., & Pizarro-Cerda, J. (2015). Genome-wide siRNA screen identifies complementary signaling pathways involved in *Listeria* infection and reveals different actin nucleation mechanisms during *Listeria* cell invasion and actin comet tail formation. *mBio*, *6*(3), e00598–15. http://doi.org/10.1128/mBio.00598-15

Leinonen, R., Akhtar, R., Birney, E., Bonfield, J., Bower, L., Corbett, M., *et al*. (2010). Improvements to services at the European Nucleotide Archive. *Nucleic Acids Research*, *38*(Database issue), D39–45. http://doi.org/10.1093/nar/gkp998

Lemaitre, B., & Girardin, S. E. (2013). Translation inhibition and metabolic stress pathways in the host response to bacterial pathogens. *Nature Reviews Microbiology*, *11*(6), 365–369. http://doi.org/10.1038/nrmicro3029

Li, W., Wang, W., Uren, P. J., Penalva, L. O. F., & Smith, A. D. (2017). Riborex: fast and flexible identification of differential translation from Ribo-seq data. *Bioinformatics*, *33*(11), 1735–1737. http://doi.org/10.1093/bioinformatics/btx047

Liao, Y., Smyth, G. K., & Shi, W. (2014). featureCounts: an efficient general purpose program for assigning sequence reads to genomic features. *Bioinformatics*, *30*(7), 923–930.

http://doi.org/10.1093/bioinformatics/btt656

Love, M. I., Huber, W., & Anders, S. (2014). Moderated estimation of fold change and dispersion for RNA-seq data with DESeq2. *Genome Biology*, *15*(12), 550. http://doi.org/10.1186/s13059-014-0550-8

Malet, J. K., Impens, F., Carvalho, F., Hamon, M. A., Cossart, P., & Ribet, D. (2018). Rapid Remodeling of the Host Epithelial Cell Proteome by the Listeriolysin O (LLO) Pore-forming Toxin. *Molecular & Cellular Proteomics*, *17*(8), 1627–1636. http://doi.org/10.1074/mcp.RA118.000767

Maury, M. M., Tsai, Y.-H., Charlier, C., Touchon, M., Chenal-Francisque, V., Leclercq, A., *et al*. (2016). Uncovering *Listeria monocytogenes* hypervirulence by harnessing its biodiversity. *Nature Genetics*. http://doi.org/10.1038/ng.3501

McGillivray, P., Ault, R., Pawashe, M., Kitchen, R., Balasubramanian, S., & Gerstein, M. (2018). A comprehensive catalog of predicted functional upstream open reading frames in humans. *Nucleic Acids Research*. http://doi.org/10.1093/nar/gky188

Mohr, I., & Sonenberg, N. (2012). Host translation at the nexus of infection and immunity. *Cell Host & Microbe*, *12*(4), 470–483. http://doi.org/10.1016/j.chom.2012.09.006

Mokrejs, M., Vopálenský, V., Kolenaty, O., Masek, T., Feketová, Z., Sekyrová, P., *et al*. (2006). IRESite: the database of experimentally verified IRES structures (www.iresite.org). *Nucleic Acids Research*, *34*(Database issue), D125–30. http://doi.org/10.1093/nar/gkj081

Neuhoff, V., Arold, N., Taube, D., & Ehrhardt, W. (1988). Improved staining of proteins in polyacrylamide gels including isoelectric focusing gels with clear background at nanogram sensitivity using Coomassie Brilliant Blue G-250 and R-250. *Electrophoresis*, *9*(6), 255–262. http://doi.org/10.1002/elps.1150090603

Niller, H. H., & Minarovits, J. (2016). Patho-epigenetics of Infectious Diseases Caused by Intracellular Bacteria. *Advances in Experimental Medicine and Biology*, *879*(2), 107–130. http://doi.org/10.1007/978-3-319-24738-0_6

Pillich, H., Chakraborty, T., & Mraheil, M. A. (2015). Cell-autonomous responses in *Listeria monocytogenes* infection. *Future Microbiology*, *10*, 583–597. http://doi.org/10.2217/fmb.15.4

Radoshevich, L., & Cossart, P. (2017). *Listeria monocytogenes*: towards a complete picture of its physiology and pathogenesis. *Nature Reviews Microbiology*, *16*(1), 32–46. http://doi.org/10.1038/nrmicro.2017.126

Ribet, D., Hamon, M. A., Gouin, E., Nahori, M.-A., Impens, F., Neyret-Kahn, H., *et al*. (2010). *Listeria monocytogenes* impairs SUMOylation for efficient infection. *Nature*, *464*(7292), 1192–1195. http://doi.org/10.1038/nature08963

Robinson, M. D., & Oshlack, A. (2010). A scaling normalization method for differential expression analysis of RNA-seq data. *Genome Biology*, *11*(3), R25–9. http://doi.org/10.1186/gb-2010-11-3-r25

Robinson, M. D., McCarthy, D. J., & Smyth, G. K. (2010). edgeR: a Bioconductor package for differential expression analysis of digital gene expression data. *Bioinformatics*, *26*(1), 139–140. http://doi.org/10.1093/bioinformatics/btp616

Sánchez-Tilló, E., Lázaro, A., Torrent, R., Cuatrecasas, M., Vaquero, E. C., Castells, A., *et al*. (2010). ZEB1 represses E-cadherin and induces an EMT by recruiting the SWI/SNF chromatin-remodeling protein BRG1. *Oncogene*, *29*(24), 3490–3500. http://doi.org/10.1038/onc.2010.102

Schwanhäusser, B., Busse, D., Li, N., Dittmar, G., Schuchhardt, J., Wolf, J., *et al*. (2011). Global quantification of mammalian gene expression control. *Nature*, *473*(7347), 337–342. http://doi.org/10.1038/nature10098

Shrestha, N., Bahnan, W., Wiley, D. J., Barber, G., Fields, K. A., & Schesser, K. (2012). Eukaryotic initiation factor 2 (eIF2) signaling regulates proinflammatory cytokine expression and bacterial invasion. *The Journal of Biological Chemistry*, *287*(34), 28738–28744. http://doi.org/10.1074/jbc.M112.375915

Sinvani, H., Haimov, O., Svitkin, Y., Sonenberg, N., Tamarkin-Ben-Harush, A., Viollet, B., & Dikstein, R. (2015). Translational tolerance of mitochondrial genes to metabolic energy stress involves TISU and eIF1-eIF4GI cooperation in start codon selection. *Cell Metabolism*, *21*(3), 479–492. http://doi.org/10.1016/j.cmet.2015.02.010

Stavru, F., Archambaud, C., & Cossart, P. (2011). Cell biology and immunology of *Listeria monocytogenes infections*: novel insights. *Immunological Reviews*, *240*(1), 160–184. http://doi.org/10.1111/j.1600-065X.2010.00993.x

Su Hui Teo, C., Serwa, R. A., & O'Hare, P. (2016). Spatial and temporal resolution of global protein synthesis during HSV infection using bioorthogonal precursors and click chemistry. *PLoS Pathogens*, *12*(10), e1005927. http://doi.org/10.1371/journal.ppat.1005927

Suzuki, Y., Chin, W.-X., Han, Q., Ichiyama, K., Lee, C. H., Eyo, Z. W., *et al*. (2016). Characterization of RyDEN (C19orf66) as an Interferon-Stimulated Cellular Inhibitor against Dengue Virus Replication. *PLoS Pathogens*, *12*(1), e1005357. http://doi.org/10.1371/journal.ppat.1005357

Tani, H., Mizutani, R., Salam, K. A., Tano, K., Ijiri, K., Wakamatsu, A., *et al*. (2012). Genome-wide determination of RNA stability reveals hundreds of short-lived noncoding transcripts in mammals. *Genome Research*, *22*(5), 947–956. http://doi.org/10.1101/gr.130559.111

Tattoli, I., Sorbara, M. T., Yang, C., Tooze, S. A., Philpott, D. J., & Girardin, S. E. (2013). *Listeria* phospholipases subvert host autophagic defenses by stalling pre-autophagosomal structures. *The EMBO Journal*, *32*(23), 3066–3078. http://doi.org/10.1038/emboj.2013.234

Weinmaier, T., Riesing, M., Rattei, T., Bille, J., Arguedas-Villa, C., Stephan, R., & Tasara, T. (2013). Complete genome sequence of *Listeria monocytogenes* LL195, a serotype 4b strain from the 1983-1987 listeriosis epidemic in Switzerland. *Genome Announcements*, *1*(1), e00152–12–e00152–12. http://doi.org/10.1128/genomeA.00152-12

Wilbertz, J. H., Voigt, F., Horvathova, I., Roth, G., Zhan, Y., & Chao, J. A. (2019). Single-Molecule Imaging of mRNA Localization and Regulation during the Integrated Stress Response. *Molecular Cell*, *73*(5), 946–958.e7. http://doi.org/10.1016/j.molcel.2018.12.006

Wu, D., Lim, E., Vaillant, F., Asselin-Labat, M.-L., Visvader, J. E., & Smyth, G. K. (2010). ROAST: rotation gene set tests for complex microarray experiments. *Bioinformatics*, *26*(17), 2176–2182. http://doi.org/10.1093/bioinformatics/btq401

Yamashita, R., Suzuki, Y., Takeuchi, N., Wakaguri, H., Ueda, T., Sugano, S., & Nakai, K. (2008). Comprehensive detection of human terminal oligo-pyrimidine (TOP) genes and analysis of their characteristics. *Nucleic Acids Research*, *36*(11), 3707–3715. http://doi.org/10.1093/nar/gkn248

Yu, G., Wang, L.-G., Han, Y., & He, Q.-Y. (2012). clusterProfiler: an R package for comparing biological themes among gene clusters. *Omics : a Journal of Integrative Biology*, *16*(5), 284–287. http://doi.org/10.1089/omi.2011.0118

Figures

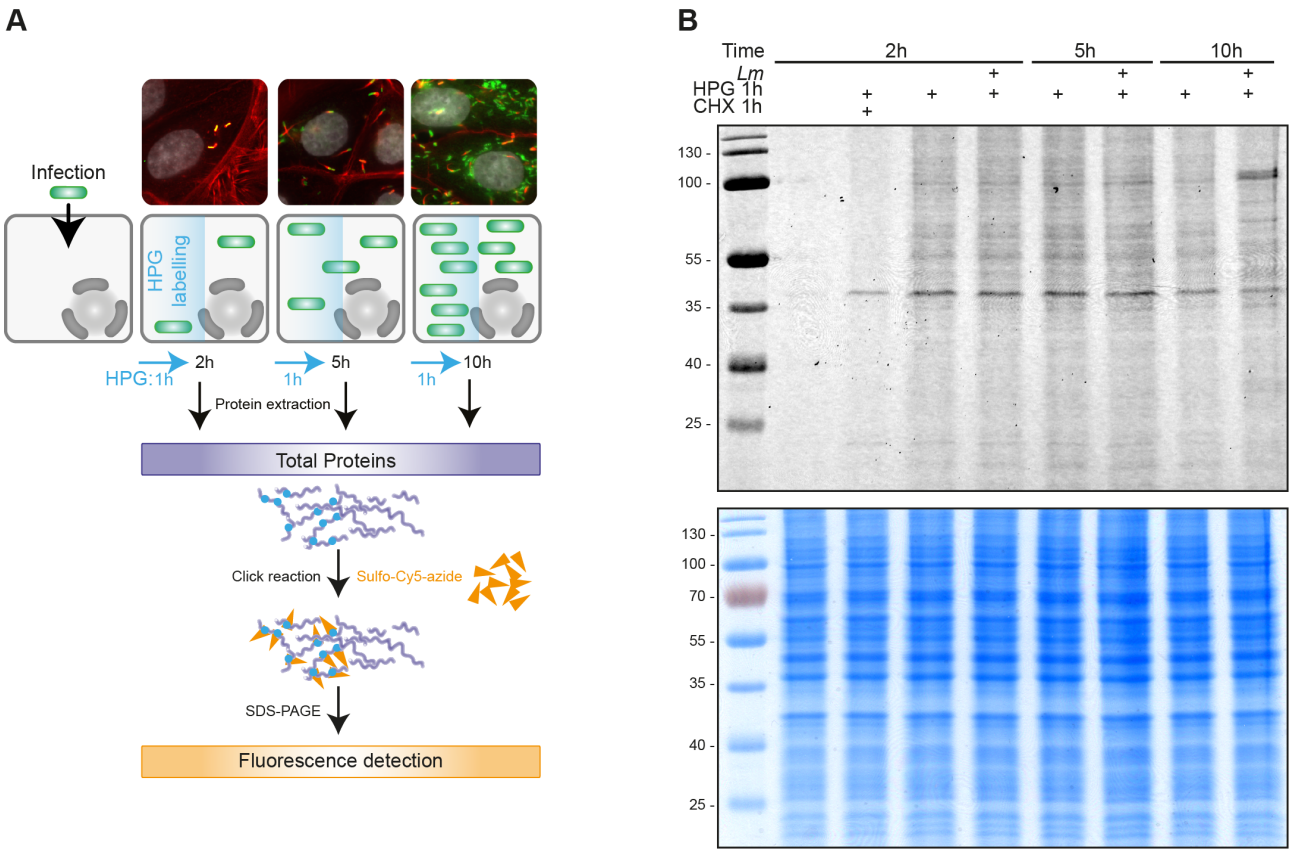

Figure 1. *Lm* infection has a low impact on total translation activity of epithelial cells. (A) Principle of the metabolic labelling of newly synthesized proteins with homopropargylglycine (HPG) over an infection time course. LoVo cells, infected or not for 2, 5 or 10 h with *Lm* LL195 constitutively expressing eGFP, were treated with HPG for 1 h prior to recovery (Su Hui Teo, Serwa, & O'Hare, 2016). Cell infection was monitored by immunofluorescence staining on coverslips. DAPI staining of cell nuclei is displayed in white, F-actin staining by fluorescently-labelled phalloidin is in red, and eGFP-expressing bacteria are in green. After cell lysis, HPG residues that had been incorporated into newly-synthesised proteins were conjugated with sulfo-Cy5-azide by copper-catalysed alkyne-azide cycloaddition. (B) In-gel fluorescence detection of HPG incorporation into newly synthesised proteins. Following cycloaddition, protein samples were separated by separated by SDS-PAGE, and Cy5 fluorescence was recorded (*top panel*), before the gel was stained with colloidal Coomassie as a loading control (*Bottom panel*).

The following figure supplement is available for figure 1:

Figure supplement 1. Assessment of infection homogeneity.

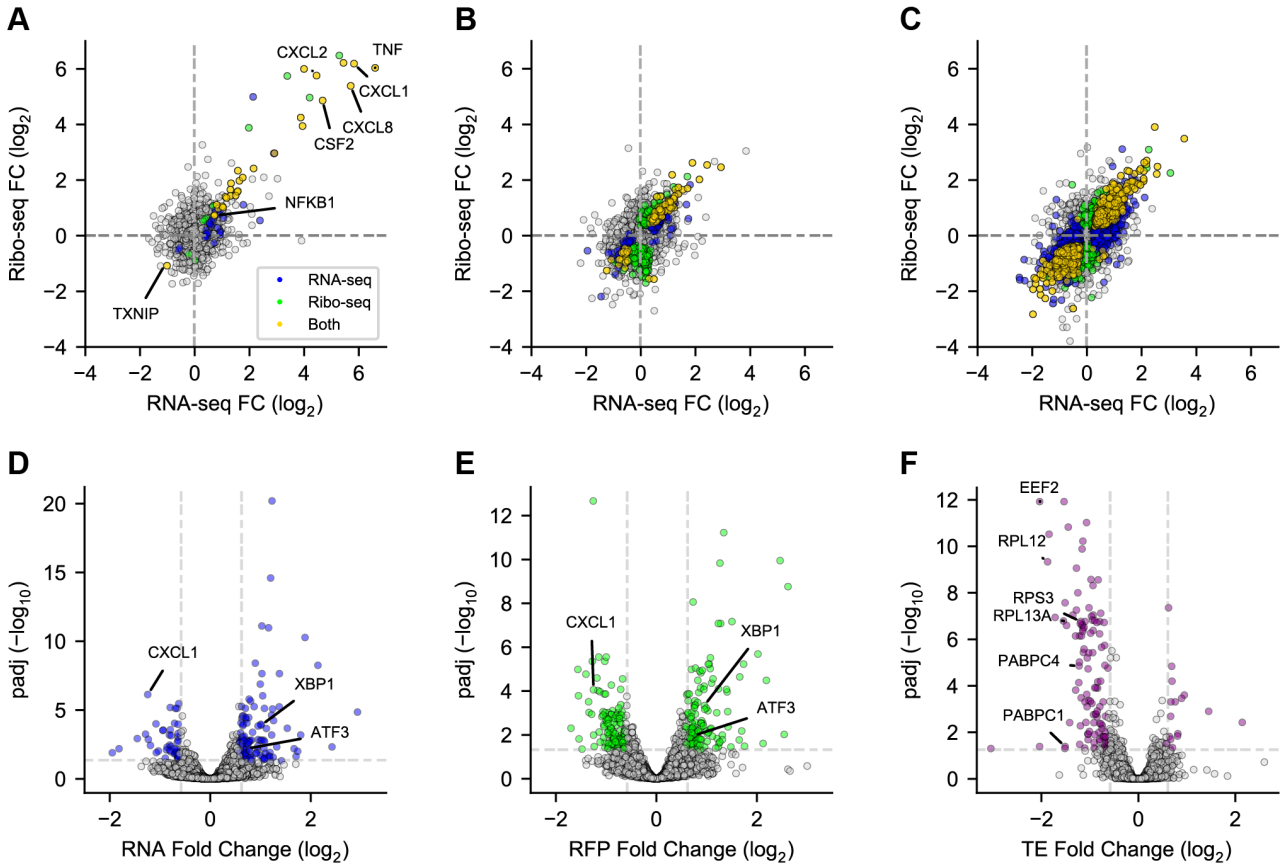

Figure 2. Transcriptional up- & translational downregulations dominate gene expression response to *Lm* in the first hours of infection. LoVo intestinal epithelial cells were infected for 2 to 10 h. Cell lysates were processed for total cytoplasmic RNA-seq and ribosome profiling (Ribo-seq). (A-C) Scatter plots of transcriptional (*Y axis*) *vs* translational (*X axis*) changes in gene expression along the course of infection, when comparing 2 h *vs* non-infected (A), 5 *vs* 2 h (B) or 10 *vs* 5 h (C). (D-E) Volcano plots highlighting genes being significantly up- (*right*) or down- (*left*) regulated in RNA-seq (D), Ribo-seq (E) or translation efficiency (F) at 5 h p.i. compared to 2 h p.i. Volcano plot coloured data points represent genes with a p adjusted value below 0.05 (above dashed grey horizontal line; $-\log_{10} p_{adj} = 1.3$) and a FC below or above 1.5 (vertical dashed grey lines; $\log_2 FC = \pm 0.58$). (A-E) Data from three independent replicates (except for RFPs at 10 h). FC, fold change; p_{adj}, adjusted *p*-value [DESeq false discovery rate (FDR)].

The following figure supplement is available for figure 2:

Figure supplement 1. Quality controls of the RNA-seq and Ribo-seq data.

The following source data will be made available for figure 2 upon full submission:

Source data 1. Source data from RNA-seq and Ribo-seq analysis used for *Figure 2*.

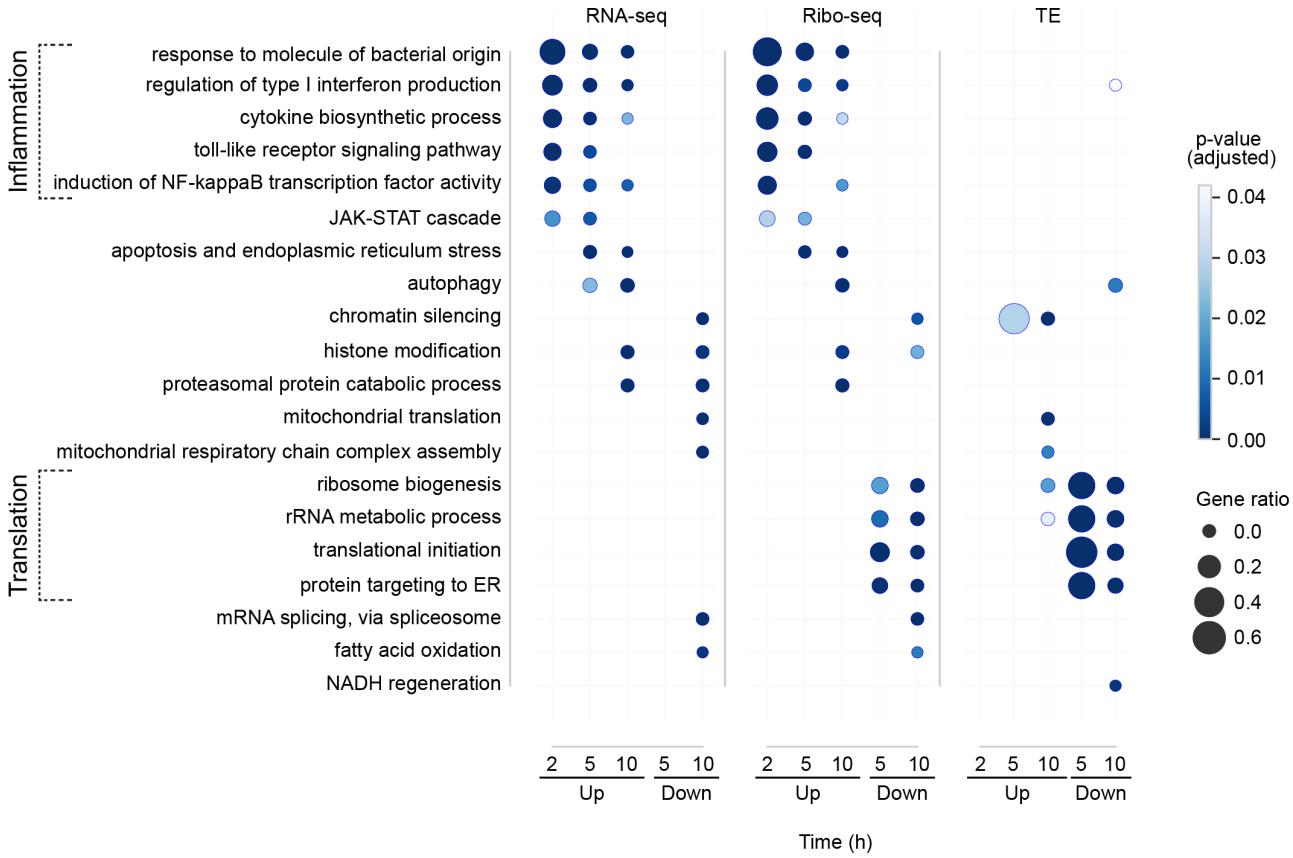

Figure 3. Early transcriptional regulation of inflammatory response precedes a translational repression of the translational equipment. Over-representation analysis of GO Biological Process terms for up- or down-regulated genes in RNA-Seq, Ribo-Seq or TE over all time points. For each time point, DRGs were selected by comparison to the non-infected condition.

The following figure supplement is available for figure 3:

Figure supplement 1. Quantification of the variation of RNA and RFP levels for ATF genes during infection.

The following source data will be made available for figure 3 upon full submission:

Source data 1. Source data from Over-representation analysis for *Figure 3*.

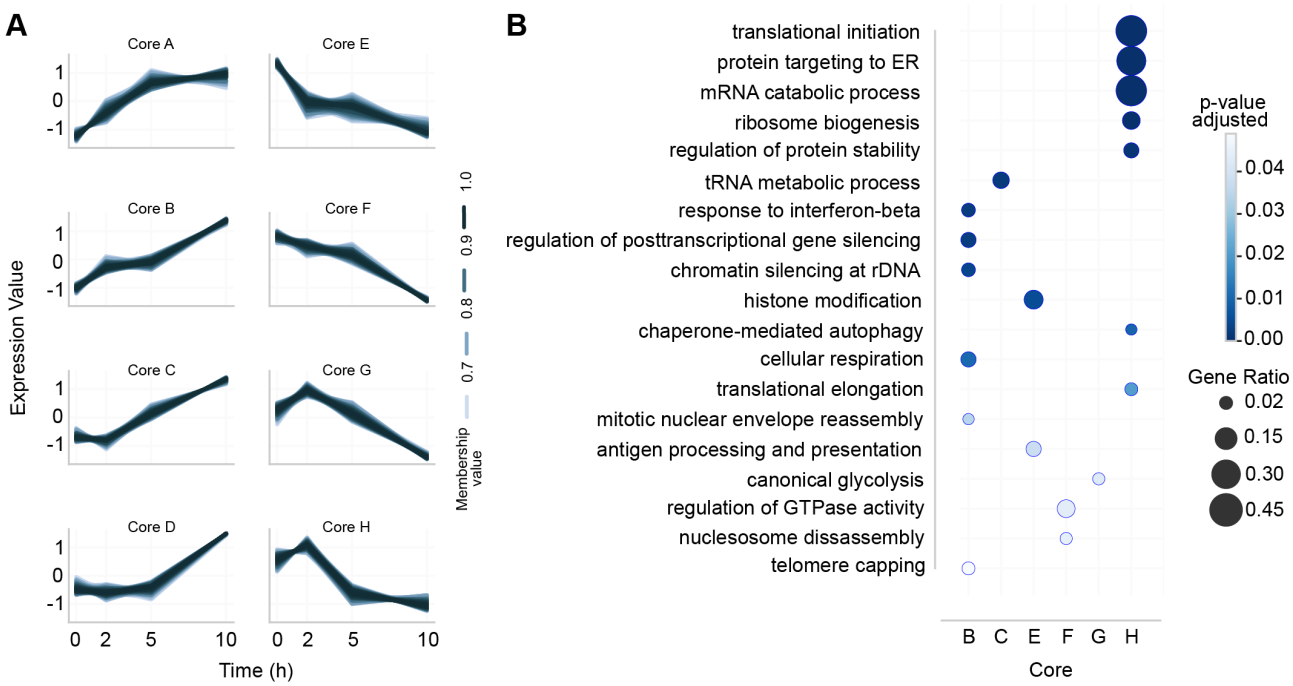

Figure 4. Translationally co-regulated genes can be grouped into functional clusters. (**A**) Transcripts sharing similar TE profiles over time were clustered by fuzzy clustering**.** For each cluster, only genes having more than 70% membership are displayed. (**B**) Functional categories were assigned to each cluster by over-representation analysis of GO Biological Process terms.

The following source data will be made available for figure 4 upon full submission:

Source data 1. Source data from fuzzy flustering for *Figure 4A*.

Source data 2. Source data from Over-representation analysis for *Figure 4B*.

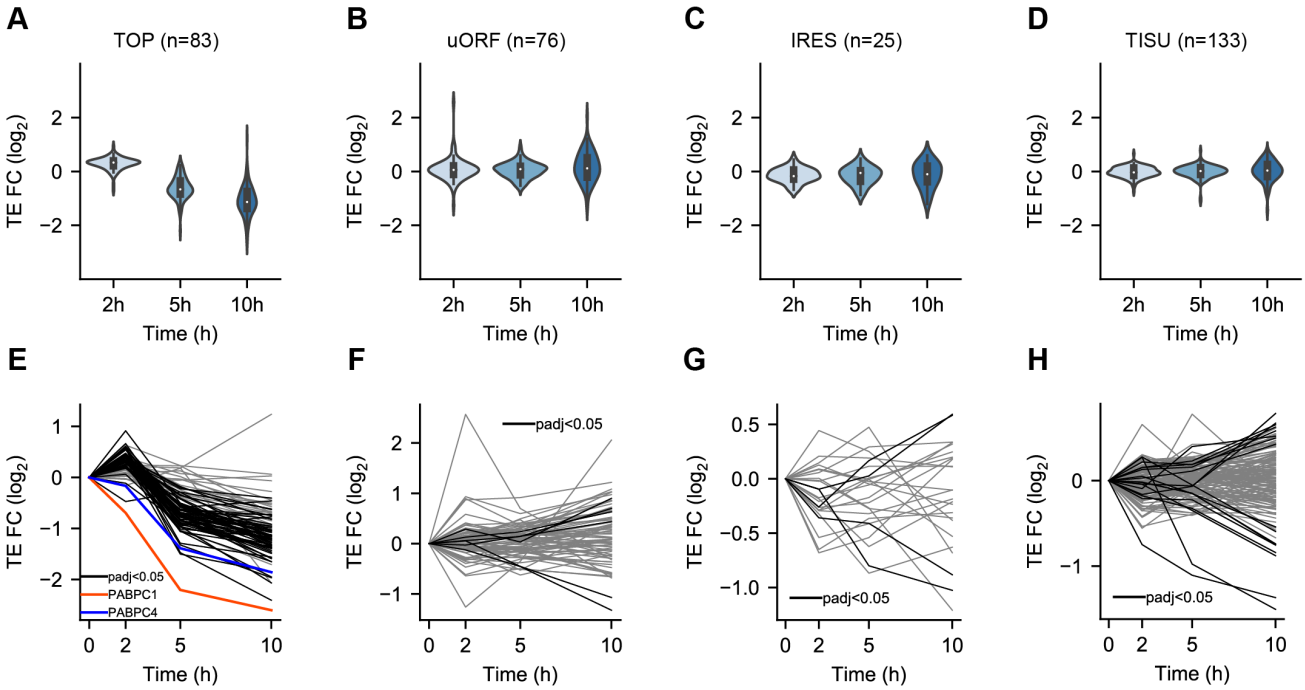

Fig. 5. 5'-terminal oligopyrimidine-containing transcripts are predominantly translationally repressed. **(A-D)** Violin plots representing fold changes in TE across time of transcripts that have been experimentally verified to contain functional TOP (**A**), uORF (**B**) or IRES (**C**) motifs, or predicted to contain a TISU (**D**), in their 5'-UTR region. (**E-H**) Translation efficiency profiles of individual transcripts containing either a TOP (**E**), uORF (**F**), IRES (**G**) or TISU (**H**) motifs. Transcripts for which the adjusted *p*-value from Riborex analysis was below 0.5 are displayed in black line (except *PABPC1* and *PABPC4*, in red and blue, respectively), while transcripts for which TE changes were not significant are displayed in grey.

The following figure supplement is available for figure 5:

Figure supplement 1. Localisation of PABPC1 mRNA in LoVo cells infected or not with *Listeria monocytogenes*.

The following source data will be made available for figure 5 upon full submission:

Source data 1. Source data from analysis of fold changes in TE for TOP-, uORF-, IRES- or TISU-containing transcripts for *Figure 5*.

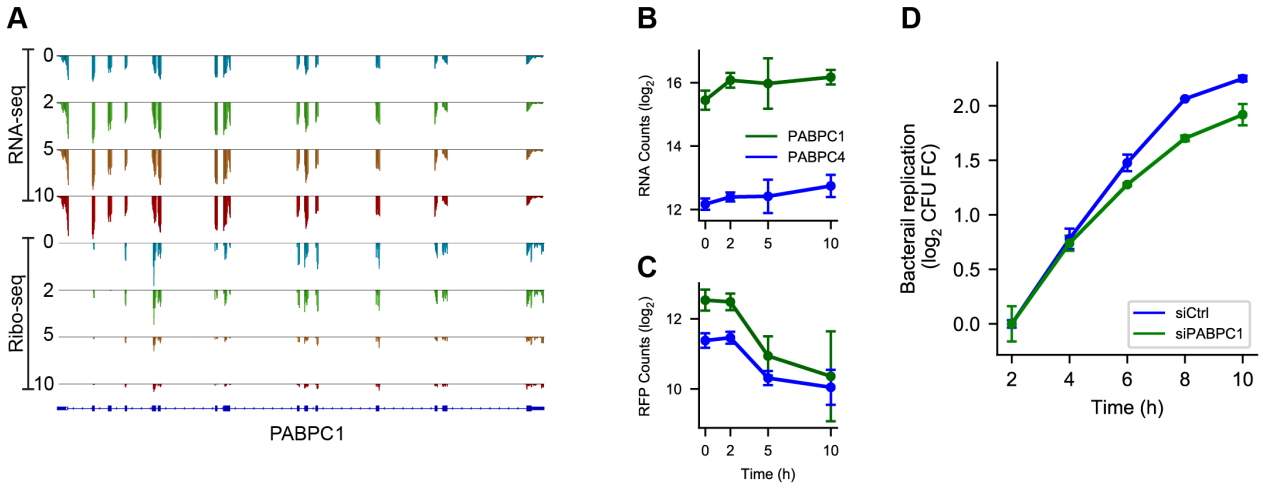

Fig. 6. Cytoplasmic poly(A)-binding protein is a regulated target during infection and an actor of the host response to infection. **(A-C)** *PABPC1* and *PABPC4* are translationally repressed during infection. (**A**) Profiles of RNA-Seq (*top*) and Ribo-Seq (*bottom*) reads aligned at the *PABPC1* locus. RPKM average values from three independent experiments, normalized for library size, are represented for each time-point. (**B-C**) Quantification of the variation of PABPC1 and PABPC4 RNA (**B**) and RFP (**C**) levels during infection. Data represent DESeq normalized counts from three independent experiments and error bars indicate standard deviation. **(D)** Silencing of *PABPC1* reduces *Lm* intracellular replication rate. LoVo cells were transfected with siRNA against PABPC1 or a scrambled siRNA (siCtrl) for 48 h before infection. Bacterial entry and replication were assessed by gentamycin-protection assay followed by serial dilution plating of infected cell lysates on agar plates. In order to focus on intracellular multiplication rather than differences in entry, the $\log_2$ ratio of colony forming units (CFU) counts at each time points relative to time 2 h post-infection were plotted. **(B-D)** Error bars indicate standard deviation (independent triplicates).

The following figure supplement is available for figure 6:

Figure supplement 1. Assessment of the efficiency of *PABPC1* silencing.

The following source data will be made available for figure 6 upon full submission:

Source data 1. Source data from DESeq analysis of fold changes in *PABPC1* and *PABPC4* RNA levels and RFPs for *Figure 6B-C*.

Source data 2. Source data from analysis of fold changes in intracellular CFU counts for *Figure 6D*.

Table 1. Oligonucleotides used in this study.

Name	Description	Sequence	Modification
oAL673	rRNA depletion	GGGGGGATGCGTGCATTTATCAGATCA	5'-biotin
oAL674	rRNA depletion	TTGGTGACTCTAGATAACCTCGGGCCGATCGCACG	5'-biotin
oAL675	rRNA depletion	GAGCCGCCTGGATACCGCAGCTAGGAATAATGGAAT	5'-biotin
oAL676	rRNA depletion	TCGTGGGGGGCCCAAGTCCTTCTGATCGAGGCCC	5'-biotin
oAL677	rRNA depletion	GCACTCGCCGAATCCCGGGGCCGAGGGAGCGA	5'-biotin
oAL678	rRNA depletion	GGGGCCGGGCCGCCCCTCCCACGGCGCG	5'-biotin
oAL679	rRNA depletion	GGGGCCGGGCCACCCCTCCCACGGCGCG	5'-biotin
oAL680	rRNA depletion	CCCAGTGCGCCCCGGGCGTCGTCGCGCCGTCGGGTCCCGGG	5'-biotin
oAL681	rRNA depletion	TCCGCCGAGGGCGCACCACCGGCCCGTCTCGCC	5'-biotin
oAL682	rRNA depletion	AGGGGCTCTCGCTTCTGGCGCCAAGCGT	5'-biotin
oAL683	rRNA depletion	GAGCCTCGGTTGGCCCCGGATAGCCGGGTCCCCGT	5'-biotin
oAL684	rRNA depletion	GAGCCTCGGTTGGCCTCGGATAGCCGGTCCCCCGC	5'-biotin
oAL685	rRNA depletion	TCGCTGCGATCTATTGAAAGTCAGCCCTCGACACA	5'-biotin
oAL686	rRNA depletion	TCCTCCCGGGGCTACGCCTGTCTGAGCGTCGCT	5'-biotin
oAL687	rRNA depletion	CATTGATCATCGACACTTCGAACGCACTTGC	5'-biotin
oAL688	rRNA depletion	ACCGCCTGGGAATACCGGGTGCTGTAGGCTT	5'-biotin
oAL689	rRNA depletion	ATTAAATCAGTTATGGTTCCTTTGGTCGCTCG	5'-biotin
oAL690	rRNA depletion	TACTTGGATAACTGTGGTAATTCTAGAGCTAATA	5'-biotin
oAL691	rRNA depletion	GCGGCGACGACCCATTCGAACGTCTGCCCTATC	5'-biotin
oAL692	rRNA depletion	AGCGTTTACTTTGAAAAAATTAGAGTGTTCA	5'-biotin
oAL693	rRNA depletion	ATAAACGATGCCGACCGGCGATGCGGCGGCGTTA	5'-biotin
oAL694	rRNA depletion	CAGTCCGCCCGGAGGATTCAACCCGGCGGCGGG	5'-biotin
oAL695	rRNA depletion	GAGCGAGCGCACGGGGTCGGCGGCGAC	5'-biotin
oAL696	rRNA depletion	TCGCCGGCCGAGGTGGGATCCCGAGGCCTC	5'-biotin
oAL697	rRNA depletion	CCCCCGCCACGCAGTTTTATCCGGTAAAGCGA	5'-biotin
oAL698	rRNA depletion	TCGTTTTTTCACTGACCCGGTGAGGCGGGG	5'-biotin
oAL699	rRNA depletion	ACCGGGGTCCGGTGCGGAGTGCCCTTCGTCC	5'-biotin
oAL700	Library PCR	AATGATACGGCGACCACCGAGATCTACACTCTTTCCCTACACGACGCTCTTCCGATCT	
oAL701	Library PCR	CAAGCAGAAGACGGCATACGAGATCGGTCTCGGCATTCCTGCTGAACCGCTCTTCCGATCT	
oAL714	Library RT	NNCTAANNNAGATCGGAAGAGCGTCGTGGATCCTGAACCGC	5'-P
oAL715	Library RT	NNCATTNNNAGATCGGAAGAGCGTCGTGGATCCTGAACCGC	5'-P
oAL716	Library RT	NNGCCANNNAGATCGGAAGAGCGTCGTGGATCCTGAACCGC	5'-P
oAL717	Library RT	NNGACCNNNAGATCGGAAGAGCGTCGTGGATCCTGAACCGC	5'-P
oAL718	Library RT	NNGGTTNNNAGATCGGAAGAGCGTCGTGGATCCTGAACCGC	5'-P
oAL719	Library RT	NNGTGGNNNAGATCGGAAGAGCGTCGTGGATCCTGAACCGC	5'-P
oAL720	Library RT	NNTCCGNNNAGATCGGAAGAGCGTCGTGGATCCTGAACCGC	5'-P
oAL721	Library RT	NNTGCCNNNAGATCGGAAGAGCGTCGTGGATCCTGAACCGC	5'-P
oAL722	Library RT	NNTATTNNNAGATCGGAAGAGCGTCGTGGATCCTGAACCGC	5'-P
oAL723	Library RT	NNTTAANNNAGATCGGAAGAGCGTCGTGGATCCTGAACCGC	5'-P

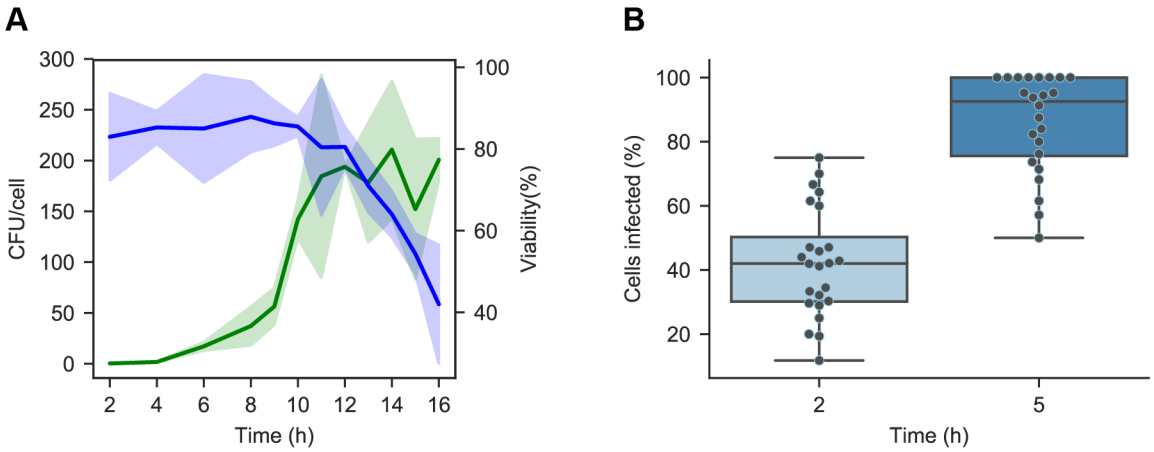

Figure 1—figure supplement 1. Assessment of infection kinetics and homogeneity. (**A**) The average number of bacteria per cell (CFU/cell, in green) and percentage of viable cells (Viability, in blue) were quantified over a 16-hour infection time course of LoVo cells, using an initial MOI of 30. CFUs were enumerated by plating serial dilutions on BHI-agar medium after cell lysis. Viability was assessed by live-dead staining using Trypan blue. Coloured bands in lighter shade indicate standard deviation. (**B**) Infection homogeneity was assessed by counting GFP-positive bacteria within each cell on microscopy slides, in 25 fields of vision per time-point. Cells were enumerated by counting DAPI-stained nuclei, and their contours were defined by revealing F-actin with Alexa Fluor 647 Phalloidin. A cell was considered infected if it contained ≥ 1 bacterial cell.

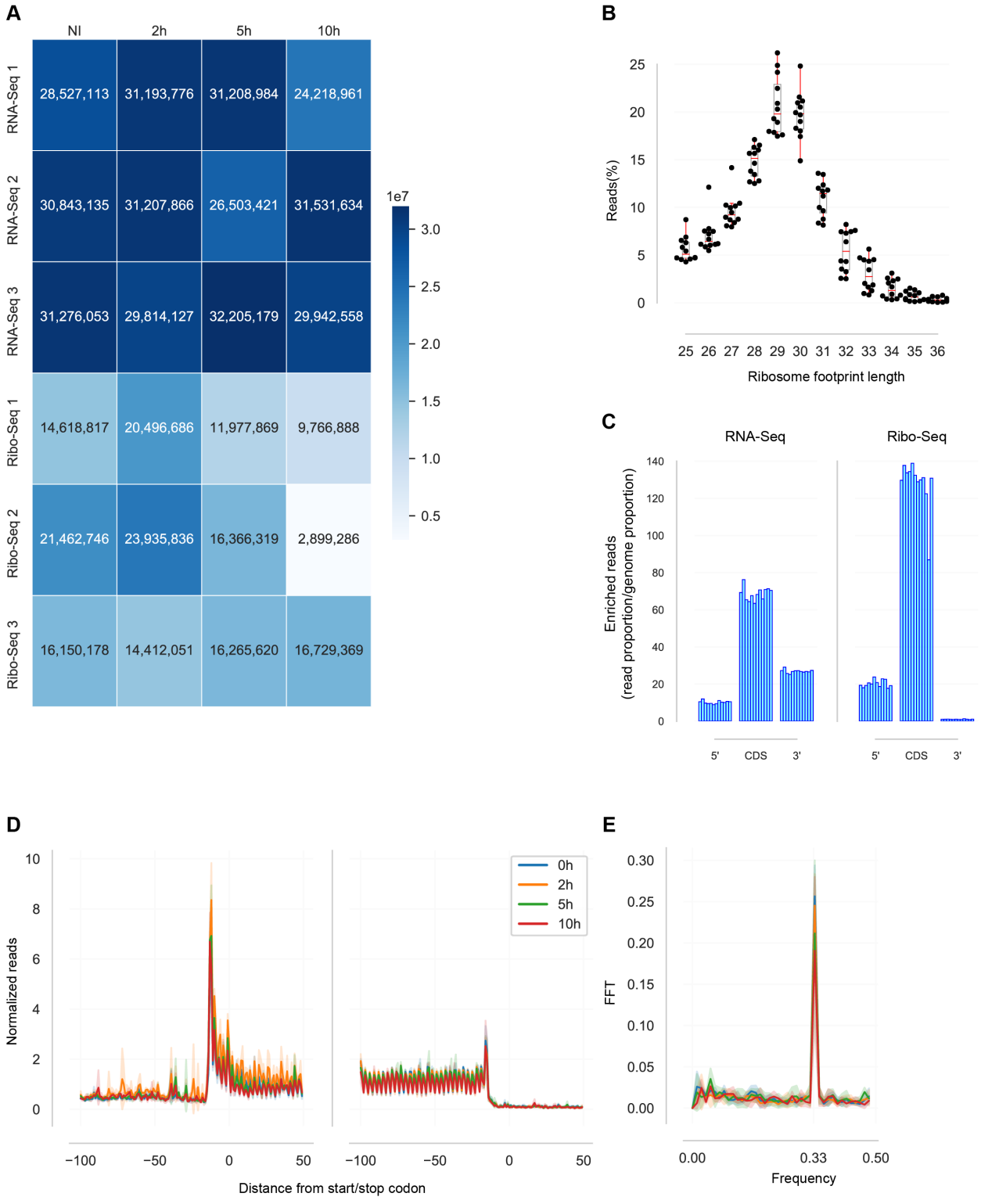

Figure 2—figure supplement 1. Quality controls of the RNA-seq and Ribo-seq data. (**A**) Number of uniquely mapped reads in each datased reported in the present study. (**B**) Distribution of RFP read length. Each dot represents one of the Ribo-seq datasets. (**C**) Proportion of uniquely mapped reads matching to 5'-UTR, coding sequences (CDS) or 3'-UTRs in all transcripts across the RNA-seq (*left*) and Ribo-seq datasets (*right*) (**D**) Position of the 5'-end of sequenced RFPs relative to translation initiation sites (TIS) and stop codons in mRNAs. For each position within a 150-nucleotide region around the TIS or the stop codon, the

counts of 5'-ends of RFP read matching this position were summed across all transcripts in each dataset and normalized by the number of transcripts. Read 5'-ends were previously reported to match around 12-13 upstream of the ribosome A site, thus the signals resulting from ribosomes scanning CDSs typically start 12 nucleotides upstream of the TIS and terminate 12 nucleotides upstream of the stop codon (Ingolia, Ghaemmaghami, Newman, & Weissman, 2009). (**E**) Codon periodicity of RFP reads in coding sequences. The signal decomposition by fast Fourier transform (FFT) of the average counts on open reading frames highlights a sharp peak at 0.33 frequency, indicative of a three-nucleotide periodicity in the RFP reads, consistent with ribosomes scanning the coding sequence during translation elongation. The colour code is as in (**D**).

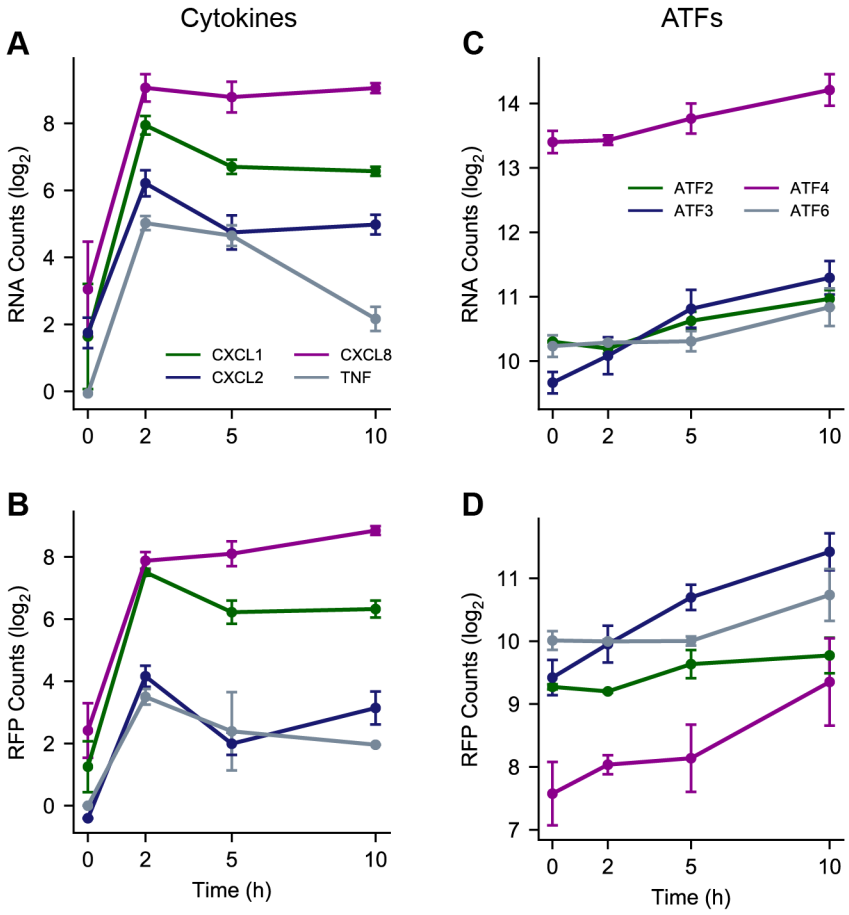

Figure 3—figure supplement 1. Quantification of the variation of RNA (**A, C**) and RFP (**B, D**) levels for selected genes related to inflammation (**A, B**) or integrated stress response (**C, D**) during infection**.** Data represent DESeq normalized read counts from three independent experiments and error bars indicate standard deviation.

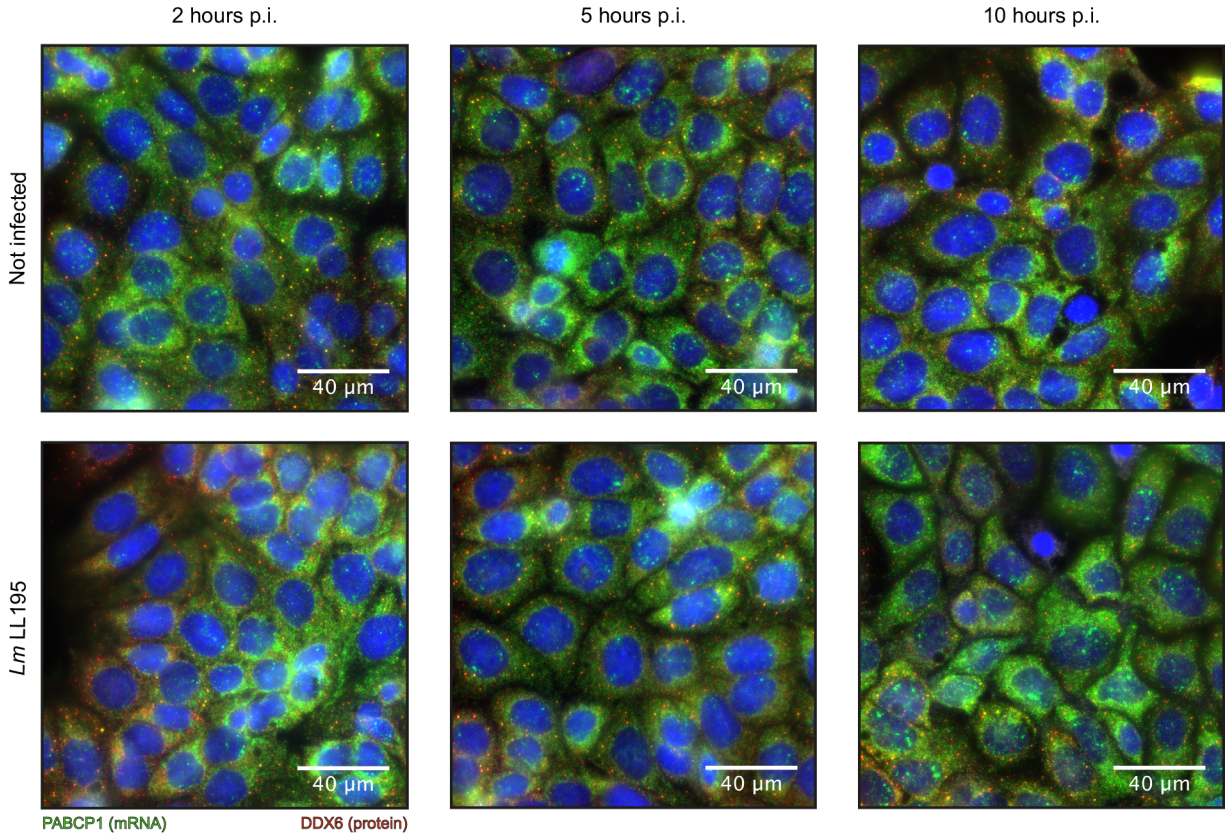

Figure 5—figure supplement 1. Localisation of PABPC1 mRNA in LoVo cells infected or not with *Listeria monocytogenes*. LoVo cells were infected with *Lm* LL195 for 2, 5 or 10 h before fixation. The localisation of PABPC1 mRNA was revealed by FISH (green), and that of P-bodies by immunofluorescence against DDX6 (red). Nuclei were stained with DAPI (blue).

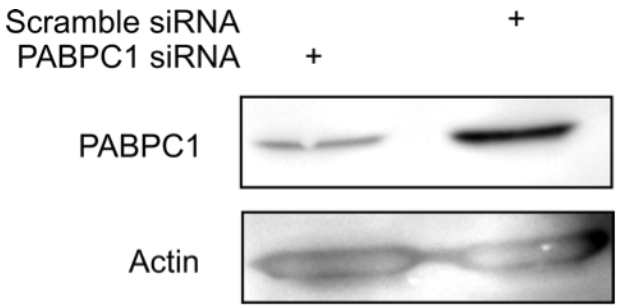

Figure 6—figure supplement 1. Assessment of the efficiency of *PABPC1* silencing. LoVo cells were transfected for 48 hours with a scramble siRNA, or siRNA against *PABPC1*. PABPC1 and actin were revealed by immunoblotting.